thermo

MDPI

Article

Thermal Performance of Galvanized-Iron Sheet Sheds with Bio-Fiber Under-Roof Insulation Mats: A Tropical Field Study

Uthra Vasudevan [1], Radhakrishnan Shanthi Priya [1,*], Geetha Ramesh Kumar [1] and Ramalingam Senthil [2]

[1] School of Architecture and Interior Design, SRM Institute of Science and Technology, Kattankulathur, Chennai 603203, India; uv0918@srmist.edu.in (U.V.); geethak@srmist.edu.in (G.R.K.)
[2] Department of Mechanical Engineering, SRM Institute of Science and Technology, Kattankulathur, Chennai 603203, India; senthilr@srmist.edu.in
* Correspondence: shanthir1@srmist.edu.in

Abstract

Galvanized iron (GI) sheets are used for temporary labor sheds in tropical regions, but they provide minimal thermal resistance. This study assessed woven grass, jute, and coir mats installed as 10 mm insulation linings beneath a corrugated 0.5 mm GI roof in Chennai, India. Four test labor sheds under one roof, separated by a shed, were compared: a bare reference and the three mats. This study measured mat properties in the laboratory, calculated U-values, and estimated roof heat flux. Hourly temperatures were recorded continuously in all four sheds from 1 to 21 May 2026. The mats lowered the calculated U-value from 4.76 W m^{-2} K^{-1} (bare sheet) to 2.17–2.44 W m^{-2} K^{-1}. On a reference day, 11 May, they reduced the peak interior-surface temperature by 1.87 to 3.13 K and the daytime-mean indoor air temperature by 1.22 to 1.92 K, with the grass mat performing best. Over the 21 measured days, the 24 h mean indoor air temperature was 0.99 to 1.64 K below the reference. Walls carried 73.5% of the calculated envelope thermal conductance, so the linings reduced envelope conductance by only 12.9% to 14.4%, and about 25 to 31 mm would be needed to meet the national roof criterion of 1.2 W m^{-2} K^{-1}. Future work should examine thicker insulation, combined roof and wall insulation, and long-term performance. It should also test different lining materials in the same shed through rotation and repeat the experiments in additional sheds using the same materials to analyze the consistency and repeatability of the results. Untreated mats should also undergo fire-safety assessment and required treatments before deployment in occupied housing.

Keywords: heat transfer; thermal resistance; thermal transmittance; transient thermal response; thermophysical properties; natural fiber insulation; lightweight metal roof; field measurement; temporary labor sheds; tropical climate

Check for updates

Academic Editor: Marcello Iasiello

Received: 9 October 2026
Revised: 19 November 2026
Accepted: 20 November 2026
Published: 22 November 2026

Copyright: © 2026 by the authors. Licensee MDPI, Basel, Switzerland. This article is an open access article distributed under the terms and conditions of the Creative Commons Attribution (CC BY) license.

1. Introduction

Cost-effective housing in India increasingly depends on affordable, climate-adapted building materials [1]. Galvanized iron (GI) sheet is a common roofing choice for transitional labor sheds because it is light, cheap, and quick to erect. A 0.5 mm steel sheet has a thermal resistance of only about 1.0×10^{-5} m^2 K W^{-1}. Its U-value therefore comes almost entirely from the surface-film resistances. Solar radiation absorbed at the outer face reaches the interior surface within minutes. These same properties make the roof thermally weak. Children in metal-roofed classrooms in tropical Africa were exposed to temperatures up to 39.8 °C, up to 5.9 °C above outdoor air [2]. The same classrooms were overheated for

72.5% of occupied hours, and a plywood ceiling beneath the metal sheet halved overheating hours [2]. In low-income urban communities, rooms with ceiling insulation were, on average, 6.9 °C cooler during the day but 1.4 °C warmer at night [3]. Insulation layers fixed beneath the roof sheet, referred to here as linings, are therefore a credible, though not an unconditional, intervention.

The thermal problem directly affects occupations in Tamil Nadu. For 1560 workers in outdoor conditions, the wet-bulb globe temperature was above 30 °C, and heat exposure was 1.4 times more likely to result in a loss of productivity [4]. Hot labs (labor sheds) that remain hot into the evening reduce recovery time after such exposure. Low-income residents consider their buildings the primary protection against heat stress, but limited low-cost materials and design constraints limit protection [5]. The roof is the most amenable retrofit area because it is horizontal, receives the most solar radiation of all envelope areas, and can be altered without affecting the structure.

Bio-insulation is appropriate for this type of building. Plant-based mats are reusable, lightweight, and can be hand-laid, and bio-based insulation composites are biodegradable and recyclable [6]. They are chemically inert and also have insulating properties due to their structure. The fibrous framework consists of cellulose and hemicellulose, and lignin stabilizes and stiffens the air in inter-fiber voids and lumens [7]. Structural models linking the thermal conductivity of bio-based foams and their structure are still difficult to apply in real systems [8]. According to ISO 8301 [9], the conductivities of coconut husk and bagasse boards ranged from 0.046 to 0.068 W m^{-1} K^{-1} [10]. Reported conductivity for straw panels ranged from 0.025 to 0.075 W m^{-1} K^{-1}, depending on the experimental method used [11]. Large uncertainties also exist for measured thermal conductivity values of bio-based building materials using the transient plane source (hot disk) method [12]. Property values shown in tables are therefore weak tools for comparing individual mats, and measured properties are better.

Studies of lightweight roofs often conflate steady-state and transient behavior. The U-value governs heat transfer under a constant temperature difference. Under the daily cycle of solar heating, heat stored in the roof layers, quantified by the areal heat capacity, lowers the amplitude of the interior-surface temperature (expressed by the decrement factor) and delays its peak (expressed by the time lag). In composite flat roofs, expanded polystyrene on the outer side and at the center plane resulted in the lowest decrement factor (0.130) [13]. In the same study, mineral wool at the center plane and on the inner side exhibited the highest time lag (9.33 h). Thin fiber mats have a much lower heat capacity, so the peak interior-surface temperature should occur at almost the same time as the peak solar heating. In 3D-printed foamed concrete, increasing porosity from 10% to 50% reduced the steady-state transmittance by 31% [14]. Linings can also reshape transient behavior: monitoring lightweight container houses over 105 days showed that an internal phase-change plaster lining reshaped heat transfer and reduced net energy exchange [15]. Calculated and in situ U-values can also diverge substantially. In situ heat flux measurements on 58 solid walls of dwellings in the United Kingdom (40 brick and 18 stone walls) yielded a mean U-value of 1.3 ± 0.4 W m^{-2} K^{-1} [16]. The typical value assumed for such solid walls was 2.1 W m^{-2} K^{-1}. Field studies are important for analyzing heat flux in lightweight roofed shelters.

Field evidence on cost-effective linings in informal housing is emerging. In two communities in Bihar, over 2 million minute-level observations showed indoor temperature reductions of 1.24 °C with radiant foils and 0.97 °C with Mylar blankets [17]. A numerical study across Indian climate zones found that straw insulation in the envelope reduced peak indoor air temperature by up to 3.5 °C in summer with the inlet temporarily closed [18]. However, existing knowledge of bio-based insulation mainly comes from material-level

tests, composite products, and simulations [19]. Temporary housing studies mostly address engineered panel systems rather than locally sourced fiber linings [20]. Thermal modeling and prototyping are also rarely applied to the cost-effective stock that houses construction labor [21]. How the response of such linings on a representative day relates to the measured mean indoor conditions over a sustained pre-monsoon hot period also remains unexamined.

The present study addresses these gaps by comparing three natural-fiber linings with a bare reference under a single roof plane. In heat-transfer terms, it separates the steady thermal resistance contributed by each lining from its transient effect on the amplitude and phase of the interior-surface temperature during periodic solar heating. The working hypothesis is that differences among grass, jute, and coir mats are small relative to experimental and property uncertainties at a fixed thickness of 10 mm. The comparison is limited to a common thickness (10 mm) because it was not possible to construct and monitor single-material linings thicker than 10 mm during the May 2026 trials. The study has the following specific objectives.

- To determine the calculated values of thermal resistance, U-value, estimated heat flux, and heat-gain reduction of 10 mm grass, jute, and coir linings under a GI roof, using measured material thermal properties and simultaneous field temperatures, compared with a reference case without lining.
- To characterize the measured 24 h diurnal response of the linings on a representative day, including amplitude attenuation, periodic dynamic characteristics, operative temperature, and overheating hours, and to quantify their measured mean response over the 21-day May 2026 monitoring period.
- To determine the envelope-level limit of a roof-only intervention through conductance decomposition, and to benchmark the results against the Eco-Niwas Samhita (ENS) roof U-value criterion and the India Model for Adaptive Comfort (IMAC).

2. Materials and Methods

2.1. Study Location and Climate Context

The field tests were conducted near Thoraipakkam on the Old Mahabalipuram Road corridor in Chennai, Tamil Nadu, India (Latitude: 12.950516° N, Longitude: 80.232039° E). The site lies about 3 km from the Bay of Bengal, within India's warm-humid climate zone. Intense construction activity along the corridor supports a large migrant workforce housed in transitional labor sheds. Monitoring took place in May 2026, the hottest pre-monsoon month, when skies are mostly clear and solar loading peaks. This period represents the most severe thermal exposure for the labor-shed stock. Figure 1 shows the study site.

2.2. Test Labor Sheds and Roof Configurations

Each test labor shed had a floor area of 19.8 m^2 (4.50 m × 4.40 m), a clear internal height of 2.50 m, and a gross wall area of 44.5 m^2. This size matches the typical single-room worker unit. A light steel frame carried a 0.5 mm GI sheet roof and uninsulated GI sheet walls. The test facility was a row of single-room labor sheds under one continuous roof plane, separated by internal GI partitions. Four units served as test labor sheds, and an empty labor shed separated each pair. Thus, no two test sheds shared a partition. In this study, a test labor shed denotes one single-room unit of the row, bounded by two partitions or by a partition and a gable wall. All test sheds therefore shared the same orientation, slope, sheet, outdoor wind, humidity, and solar exposure. Figure 2 shows the test site and the three mat materials.

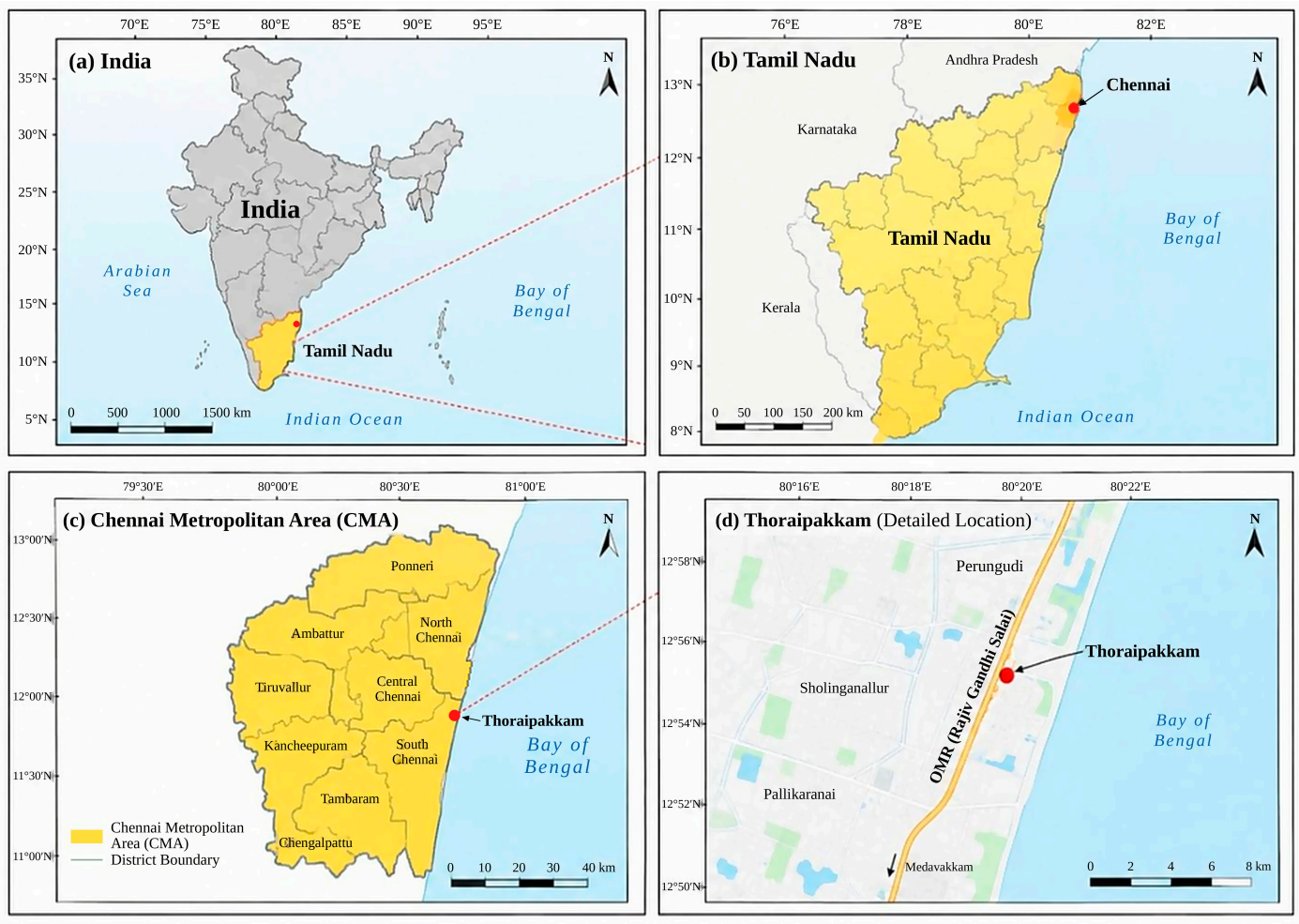
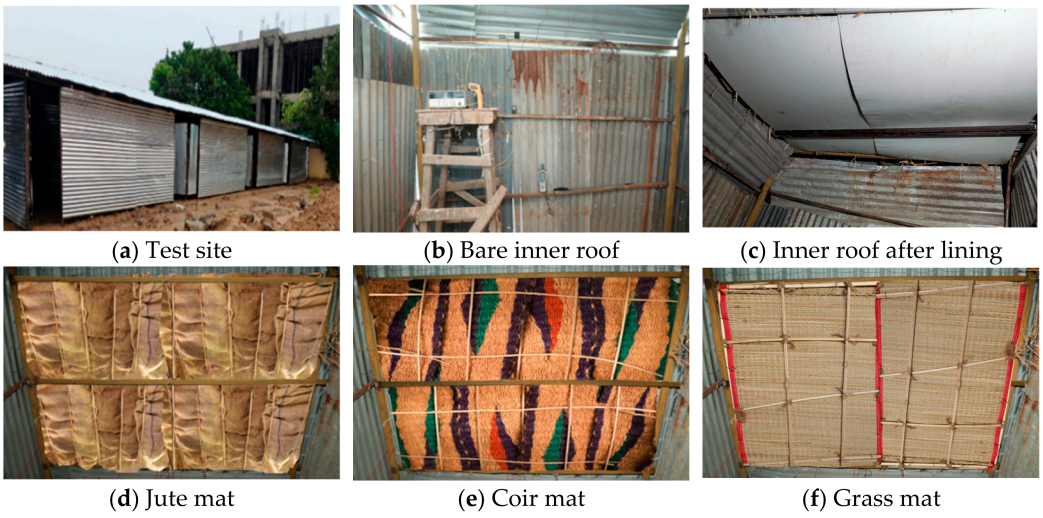


Figure 1. Location of the study site within India (**a**), Tamil Nadu (**b**), and the Chennai Metropolitan Area (**c**), with Thoraippakkam (**d**) on the Old Mahabalipuram Road corridor. The highlighted area in each panel is enlarged in the next.



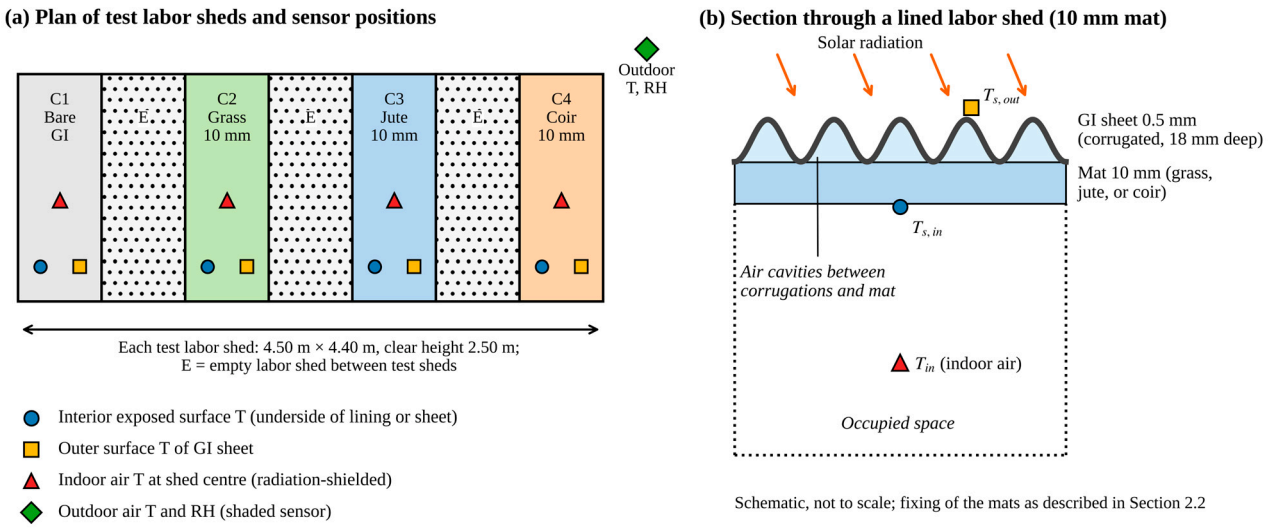
(**a**) Test site (**b**) Bare inner roof (**c**) Inner roof after lining

(**d**) Jute mat (**e**) Coir mat (**f**) Grass mat

Figure 2. Test site, bare inner roof, lined inner roof, and the three mat materials assessed.

Four roof configurations were installed, each in a separate test labor shed (Figure 3). Configuration C1 was the bare GI sheet reference. Configurations C2, C3, and C4 carried a single 10 mm woven grass, jute, or coir mat, respectively, fixed beneath the sheet as described

below. All four test labor sheds were monitored simultaneously, so the comparison is free of day-to-day weather variation, such as wind speed, humidity, and solar radiation.



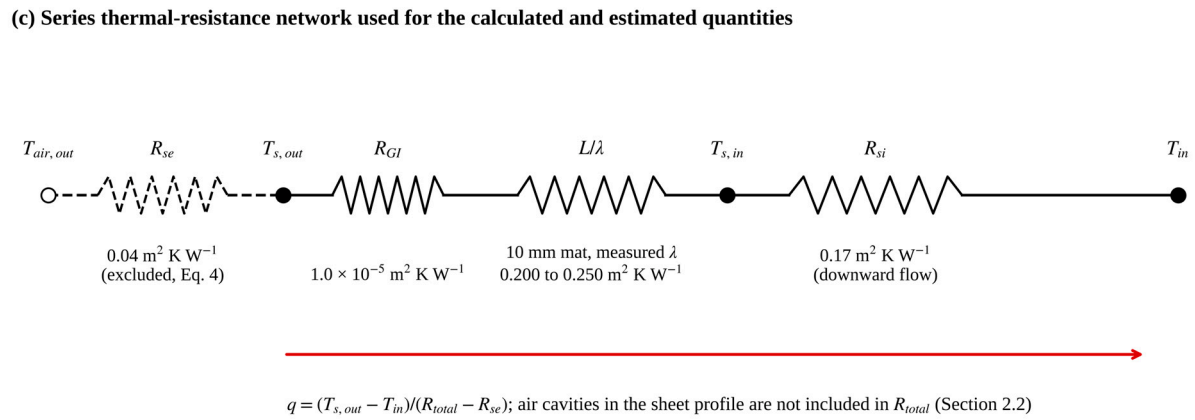


Figure 3. Experimental arrangement: (**a**) plan of the four test labor sheds, separated by empty sheds, with sensor positions, (**b**) schematic section through a lined labor shed showing the corrugated sheet, the air cavities between the corrugations and the 10 mm mat, and the sensor locations, and (**c**) series thermal-resistance network used for the calculated and estimated quantities. The red line indicates the heat-flow direction.

Heat and air can still pass from a test labor shed into the neighboring empty sheds through the partitions and through gaps between the partitions and the corrugated sheet. The empty sheds reduce, but do not remove, exchange between treatments. This exchange may make the measured differences between sheds smaller or larger than they would be in fully separated rooms; which occurs is unknown, and neither is assumed here. C1 occupied an end position of the row and is therefore the only analyzed shed with a gable wall, whereas C2 to C4 lay between empty sheds. Additional gable-wall gains would make C1 warmer and could enlarge the measured reductions, so orientation-dependent wall gains remain a possible bias in the between-shed comparison.

The roof and walls were made of corrugated, not flat, GI sheet (Figure 2b,c). The 0.5 mm value used throughout is the steel thickness; the roof profile was sinusoidal with a depth of 18 mm and a pitch of 76 mm. The mats were flat and were fixed to the underside of the sheet by binding wire to the purlins at a spacing of around 2 mm. Because a flat mat cannot follow the corrugations, it touched the sheet only along the lower crests of the profile, leaving enclosed air cavities between the sheet and the mat, up to 18 mm deep,

equal to the profile depth (Figure 3b). At the eaves and the ridge, these cavities were open to outdoor air. The $T_{s,out}$ thermocouple was fixed on a trough of the profile, and the $T_{s,in}$ thermocouple was fixed relative to the corrugations on the room side of the mat. Section 2.7 discusses how the cavities affect the calculated resistances.

The sheds were not airtight rooms. Air could move between each test shed and the neighboring empty sheds through gaps at the partition–sheet junctions or openings above the partitions, and between the sheds and outdoors through eave gaps, the door, and window openings. During monitoring, the door and the windows were kept closed. Air-change rates and airflow between sheds were not measured. Because the sheds exchange air through the intervening empty units, their indoor air temperatures are not fully independent, and differences in T_{in} are differences between partly coupled zones. The interior-surface temperature $T_{s,in}$, which depends mainly on the lining directly above the sensor, is less affected by this mixing and therefore forms the primary basis for the between-shed comparison.

2.3. Measurement of Thermophysical Properties

The thermophysical properties of the three mats (coir, grass, and jute) were measured using specimens taken from the same batches installed in the labor sheds. Thermal conductivity, λ, was determined using a guarded hot-plate apparatus (Elshaddai Engineering Equipments, ELSHADDAI–HMT–033, Chennai, India; https://elshaddaiengg.com (accessed on 27 October 2026)) under steady-state conditions, in accordance with ISO 8302 [22]. Bulk density was determined from the specimen mass and measured dimensions after conditioning. Specific heat capacity was measured using a DSC214 Polyma differential scanning calorimeter (NETZSCH-Gerätebau GmbH, Selb, Germany; https://www.netzsch.com (accessed on 27 October 2026)) following ASTM E1269 [23]. Mat thickness was measured at multiple locations using a thickness gauge (Sudershan Measuring and Engineering Pvt. Ltd., New Delhi, India; https://www.portable-testers.com (accessed on 27 October 2026) under a specified contact pressure, and the mean value was reported. Porous, hygroscopic mats gain conductivity and heat capacity with moisture, so the values apply only to the stated conditioning state. Table 1 summarizes the thermophysical properties of the roof materials.

Table 1. Thermophysical properties of the roof materials.

Material	Form	Thickness, L (mm)	Bulk Density, ρ (kg m^{-3})	Thermal Conductivity, λ (W m^{-1} K^{-1})	Specific Heat Capacity, c_p (J kg^{-1} K^{-1})	Thermal Diffusivity, α (m^2 s^{-1})	Areal Mass (kg m^{-2})	Thermal Resistance, R (m^2 K W^{-1})
GI sheet	Sheet	0.5	7850	50.0	490	1.30×10^{-5}	3.93	1.0×10^{-5}
Grass mat	Woven	10	135	0.045	2100	1.59×10^{-7}	1.35	0.222
Jute mat	Woven	10	100	0.040	1500	2.67×10^{-7}	1.00	0.250
Coir mat	Woven	10	120	0.050	1670	2.49×10^{-7}	1.20	0.200

2.4. Field Instrumentation

K-type thermocouples were connected to a multi-channel data logger (model 34970A; Agilent Technologies, Santa Clara, CA, USA). Each test labor shed carried three sensors (Figure 3). The first recorded the outer surface temperature of the GI sheet, $T_{s,out}$. The second recorded the interior exposed surface temperature, $T_{s,in}$, on the underside of the lining (or the sheet in C1). The third recorded indoor air temperature, T_{in}, at the shed center, shielded from direct radiation. A temperature and relative-humidity sensor with its own data logger, placed in a radiation shield outside the labor sheds, recorded outdoor air temperature and relative humidity. Before installation, all thermocouples were checked

against a reference thermometer. Irradiance was common across all sheds, so it did not affect comparisons between sheds.

The ISO 9869-1 average method assumes quasi-steady conditions and a test of 72 h or more [24]. This assumption is not met with a large diurnal temperature range and potentially reversed heat flow at night in a solar-driven sheet roof system. Even on a purpose-built test wall in winter, the average method deviated from the theoretical R-value by 9.12% [25]. A heat-flux plate placed on a 10 mm fibrous mat would also affect the measured surface due to the additional contact resistance and the different radiative properties of the plates and mats. Roof heat flux is therefore treated as an estimate throughout, and the calculated U-values are not independently verified.

2.5. Monitoring Period and Data Processing

The analysis is based on 21 days in May 2026. First, 11 May 2026 is identified as a representative day, and a 24 h analysis of all test labor sheds is reported at hourly time steps. The remaining 20 measured days are summarized as daily values and period means. This day was selected because all channels were complete over the 24 h, there was no rain, and the outer-surface temperature showed a smooth, single-peak profile characteristic of clear-sky conditions. Its outdoor diurnal range of 10.5 K was within 0.4 K of the 21-day mean of 10.2 K, and its daily maximum and minimum (40.2 and 29.7 °C) lay 0.7 and 1.1 K below the 21-day means. The day therefore represents typical, slightly milder-than-average loading. Daily outdoor maximum and minimum air temperatures were measured at the site.

Two temperature statistics are distinguished. The peak interior-surface temperature is the maximum hourly value of $T_{s,in}$, which was recorded at the 13:00 h reading in all sheds. With hourly logging, the true maximum can only be located to within about ±30 min of that reading. The common 13:00 h reading therefore does not show that all sheds peaked at the same moment, and differences in peak time shorter than 1 h cannot be resolved (Section 3.2). The daytime means of $T_{s,out}$ and T_{in} were computed over 06:00 to 18:00 h, and their difference forms the driving temperature difference used in the heat-flux estimate. An instantaneous peak is never used as a period mean. Daily means for the 21-day summary are taken over 00:00 to 23:00 h (24 values), so that midnight is not counted twice. To relate the response to occupancy, the 24 h record was divided into four periods. These were night (00:00 to 05:00 h), morning (06:00 to 11:00 h), afternoon (12:00 to 17:00 h), and evening (18:00 to 23:00 h).

2.6. Classification of Reported Quantities

Table 2 shows that the reported quantities differ in evidential status. Temperatures and material properties are measured. Resistance, U-value, and conductance are calculated from measured properties and standard surface resistances. Heat flux and heat-transfer rate are estimated by combining measured temperatures with calculated resistances. Mean radiant and operative temperatures are estimated from surface temperatures and a calculated ceiling angle factor. Hourly temperatures were measured over 21 days.

Table 2. Evidential status of the reported quantities.

Status	Quantities	Basis
Measured (field)	$T_{s,out}$, $T_{s,in}$, T_{in}, outdoor air temperature and relative humidity	K-type thermocouples, capacitive humidity logger
Measured (laboratory)	λ, ρ, c_p, L	Guarded hot plate method, gravimetric method, differential scanning calorimetry, thickness gauge

Table 2. *Cont.*

Status	Quantities	Basis
Calculated	R_{total}, U, α, κ, τ, UA	Equations (1)–(3), (7), (8) and (12) with measured properties and ISO 6946 surface resistances
Estimated	q, Q, HGR	Equations (4)–(6) with measured temperatures and calculated resistances
Estimated	T_{mrt}, T_{op}	Equations (10) and (18) with measured surface temperatures and a calculated ceiling angle factor
Calculated	f_d, Δt_φ, E_{st}, ε_{st}	Equations (14)–(17) with measured properties, measured swings, and ISO 13786

2.7. Thermal Performance Calculations

The U-value is treated as a steady-state comparative property of each roof assembly. The measured diurnal temperatures, by contrast, describe transient field behavior under solar loading. The two are reported separately and are not interchangeable. Steady-state resistance was calculated using the method in ISO 6946 [26]. The total resistance is the sum of the surface resistances and the layer resistances in series, as given in Equation (1).

$$R_{total} = R_{si} + \sum_{i=1}^{n} \frac{L_i}{\lambda_i} + R_{se} \quad (1)$$

For downward heat flow through a sun-exposed roof, the tabulated surface resistances are 0.17 m^2 K W^{-1} internally and 0.04 m^2 K W^{-1} externally. The U-value follows from Equation (2) [26].

In the series model of Equation (1), each mat is assumed to be in full contact with the sheet, and the air cavities between the corrugated sheet and the mats, mentioned in Section 2.2, are not considered. If the cavities are closed, ISO 6946 assigns an unventilated air layer an additional thermal resistance of 0.11 to 0.19 m^2 K W^{-1} for downward heat flow and thicknesses of 5 to 25 mm [26]. The cavity depth is not uniform across the profile, so the added resistance would be lower than these values, and it would apply only to the three lined sheds, not to C1. The calculated U-values of the lined roofs are therefore conservative if the cavities are closed. If the cavities are open at the eaves, outdoor air can carry away part of the heat absorbed by the sheet. ISO 6946 treats such a cavity as a slightly or well-ventilated air layer, making the calculated U-values less reliable. By contrast, the measured temperatures were recorded on the assemblies as installed and therefore include the cavity effect.

$$U = \frac{1}{R_{total}} \quad (2)$$

Thermal diffusivity characterizes how quickly a temperature disturbance propagates through a layer. It was obtained from the measured properties using Equation (3) [27].

$$\alpha = \frac{\lambda}{\rho c_p} \quad (3)$$

Roof heat flux was estimated from the daytime-mean outer-surface temperature and the daytime-mean indoor air temperature. Because $T_{s,out}$ is measured, the external surface resistance is excluded from the denominator, consistent with the in situ convention of ISO 9869-1 [24]. The measured outer-surface temperature already embeds absorbed solar radiation, external convection, and long-wave exchange with the sky. These terms are therefore not modeled separately. The estimate covers conduction through the assembly

and combined convective and radiative transfer at the interior surface, represented by R_{si}. Equation (4) gives the estimated flux.

$$q = \frac{T_{s,out} - T_{in}}{R_{total} - R_{se}} \tag{4}$$

The roof heat-transfer rate follows from Equation (5) [27]. It is a daytime-mean estimate, not an instantaneous peak. For comparability, each configuration is expressed over the full 19.8 m^2 roof, as if that lining covered the entire roof.

$$Q = qA_{roof} \tag{5}$$

Heat gain reduction (HGR) is the ratio of the estimated reduction in roof heat flux to the reference value, defined by Equation (6) in this study. It is expressed as a heat-flux ratio because a temperature ratio is not a ratio of energy transferred and depends on the arbitrary zero of the Celsius scale.

$$HGR = \frac{q_{ref} - q_{config}}{q_{ref}} \times 100 \tag{6}$$

The areal heat capacity of each assembly was calculated as the sum of the layer heat capacities, following ISO 13786 [28], as given in Equation (7).

$$\kappa = \sum_{i=1}^{n} \rho_i c_{p,i} L_i \tag{7}$$

A thermal time constant was then obtained from Equation (8). It treats the whole assembly as a single heat capacity charged through its total resistance, which is the lumped-capacitance approximation of transient conduction [27]; it is referred to below as the single-capacity time constant. This quantity indicates thermal inertia to within an order of magnitude. It is not the periodic time shift defined in ISO 13786, which requires the full transfer-matrix solution.

$$\tau = R_{total}\kappa \tag{8}$$

The measured diurnal swing of the interior-surface temperature was referenced to the bare GI labor shed using Equation (9). This study defines the ratio by analogy with the decrement factor in ISO 13786 [28], but it uses measured surface temperatures rather than a calculated transmittance.

$$f = \frac{T_{max} - T_{min}}{T_{max,ref} - T_{min,ref}} \tag{9}$$

Operative temperature is important in a radiatively dominated enclosure. Equation (10) combines air temperature and mean radiant temperature (MRT), weighted by the convective and radiative coefficients as defined in ISO 7726 [29]. At the low air speeds in the labor sheds, the convective and radiative heat transfer coefficients are similar, so operative temperature approaches the mean of the two.

$$T_{op} = \frac{h_c T_{air} + h_r T_{mrt}}{h_c + h_r} \tag{10}$$

Indoor conditions were compared with IMAC, whose neutral temperature for naturally ventilated buildings is given by Equation (11) [30]. The 90% and 80% acceptability bands are ±2.4 K and ±4.1 K, respectively. The model applies to 30-day outdoor running means of 12.5 to 31 °C. This study calculated the actual outdoor mean using Equation (19) in Section 2.9. Because it exceeded the 31 °C applicability limit, the neutral temperature was evaluated at that limit.

$$T_n = 0.54T_{rm} + 12.83 \tag{11}$$

The roof contribution to the envelope was determined from the envelope conductance in Equation (12), which is the transmission heat transfer coefficient of ISO 13789 [31] restricted to the roof and walls. The floor was excluded because it is a ground-coupled heat sink rather than a solar-gain path.

$$UA_{env} = U_{roof}A_{roof} + U_{wall}A_{wall} \tag{12}$$

2.8. Uncertainty Analysis

Uncertainties in derived quantities were propagated using Moffat's root-sum-square method [32], as shown in Equation (13).

$$\Delta Y = \sqrt{\sum_{i=1}^{n}\left(\frac{\partial Y}{\partial X_i}\Delta X_i\right)^2} \tag{13}$$

The uncertainty in the total resistance arises from four factors: layer thickness, measured conductivity, surface-film resistance, and interfacial contact resistance. These are propagated to the U-value, heat flux, and HGR. Table 3 gives the elemental values. The conductivity uncertainty combines the instrument uncertainty from the guarded hot plate method and specimen-to-specimen variability. The combined uncertainty for the temperature difference between two sensors is ±0.42 K. This bound is a measurement-resolution criterion, not a statistical equivalence test.

Table 3. Measured quantities and elemental uncertainties adopted for the propagation analysis.

Quantity	Instrument or Source	Elemental Uncertainty
Air and surface temperature	K-type thermocouple with multi-channel logger	±0.3 °C
Relative humidity	Capacitive logger	±2.5%
Layer thickness	Thickness gauge	±0.5 mm
Thermal conductivity	Guarded hot plate method	±2%
Roof area	Steel tape	±1%
Surface-film resistances	ISO 6946 tabulated values	±0.014 m^2 K W^{-1}
Interfacial contact resistance	Literature estimate	±0.02 m^2 K W^{-1}

2.9. Dynamic and Comfort Evaluation Methods

Equation (4) neglects heat stored in the assembly. The energy stored per unit area during the diurnal rise was estimated from the areal heat capacity and the measured diurnal swing of the interior-surface temperature, as given in Equation (14) [27]. Its share of the daytime conducted energy follows from Equation (15), defined for this study, with $\Delta t_d = 12$ h.

$$E_{st} = \kappa \Delta T_{sw} \tag{14}$$

$$\varepsilon_{st} = \frac{E_{st}}{q\Delta t_d} \times 100 \tag{15}$$

The periodic response was calculated with the transfer-matrix method of ISO 13786 [28] for a 24 h period. The decrement factor and the periodic time shift follow from the periodic thermal transmittance $Y_{12} = -1/Z_{12}$, as given in Equations (16) and (17).

$$f_d = \frac{|Y_{12}|}{U} \tag{16}$$

$$\Delta t_\varphi = \frac{P}{2\pi}\arg(Y_{12}) \tag{17}$$

Mean radiant temperature at the shed center was estimated from Equation (18). The ceiling angle factor $F_c = 0.14$ was calculated for a seated person at the center of the 4.50 m × 4.40 m ceiling, 1.9 m below it, using the angle-factor relations of ISO 7726 [29]. The other surfaces were assigned the indoor air temperature because wall surface temperatures were not measured, which underestimates the radiant load from the hot GI walls. Operative temperature then follows from Equation (10) with $h_c \approx h_r$. Overheating hours were counted as hours in which the estimated operative temperature exceeded the upper IMAC 80% limit.

$$T_{mrt} = F_c T_{s,in} + (1 - F_c) T_{in} \quad (18)$$

IMAC defines its running mean over the preceding 30 days [30]. Outdoor records before 1 May 2026 were unavailable, so this study used the arithmetic mean of daily outdoor temperatures over the available days, as in Equation (19), with $T_{od,i}$ taken as the mean of the daily maximum and minimum.

$$T_{rm} = \frac{1}{n} \sum_{i=1}^{n} T_{od,i} \quad (19)$$

3. Results and Discussion

3.1. Measured Temperatures

Table 4 and Figure 4 summarize the measured temperatures on 11 May 2026. The daytime-mean outer-surface temperature varied by only 0.07 K across the four test labor sheds (40.99 to 41.06 °C). This confirms that the sheds experienced near-identical external exposure. The peak interior-surface temperature of the bare GI shed was 45.10 °C, and its daytime-mean indoor air temperature was 35.47 °C, which gives a driving temperature difference of 9.63 °C between the outer surface and the indoor air.

Table 4. Measured temperatures of the four roof configurations on 11 May 2026.

Configuration	$T_{s,out}$ (°C)	Peak $T_{s,in}$ (°C)	T_{in} (°C)	ΔT (K)	Peak $T_{s,in}$ Reduction (K)	T_{in} Reduction (K)
GI sheet (reference)	41.06	45.10	35.47	5.59	0.00	0.00
Grass mat (10 mm)	40.99	41.97	33.55	7.45	3.13	1.92
Jute mat (10 mm)	41.03	42.70	34.06	6.97	2.40	1.41
Coir mat (10 mm)	40.99	43.23	34.25	6.75	1.87	1.22

All three linings reduced the maximum temperature on the interior surfaces. The reductions were 3.13 K for grass, 2.40 K for jute, and 1.87 K for coir, respectively. The 0.73 K separation between grass and jute and the 0.53 K separation between jute and coir exceed the resolution limit of ±0.42 K; thus, the surface temperature measurements for this day rank the mats as grass, jute, and coir. This ranking is based on one shed per treatment. The 21-day means in Section 3.8 show the same order, but neither equivalence nor general superiority is established.

Indoor air temperature followed the same order with a compressed spread. The daytime-mean values were 33.55, 34.06, and 34.25 °C for grass, jute, and coir, or 1.92, 1.41, and 1.22 K below the reference. The 0.70 K spread between grass and coir exceeds the combined uncertainty, whereas the 0.19 K difference between jute and coir does not. The driving temperature difference rose from 5.59 K in the reference to 6.75–7.45 K in the lined sheds because the linings retained more heat above the occupied zone.

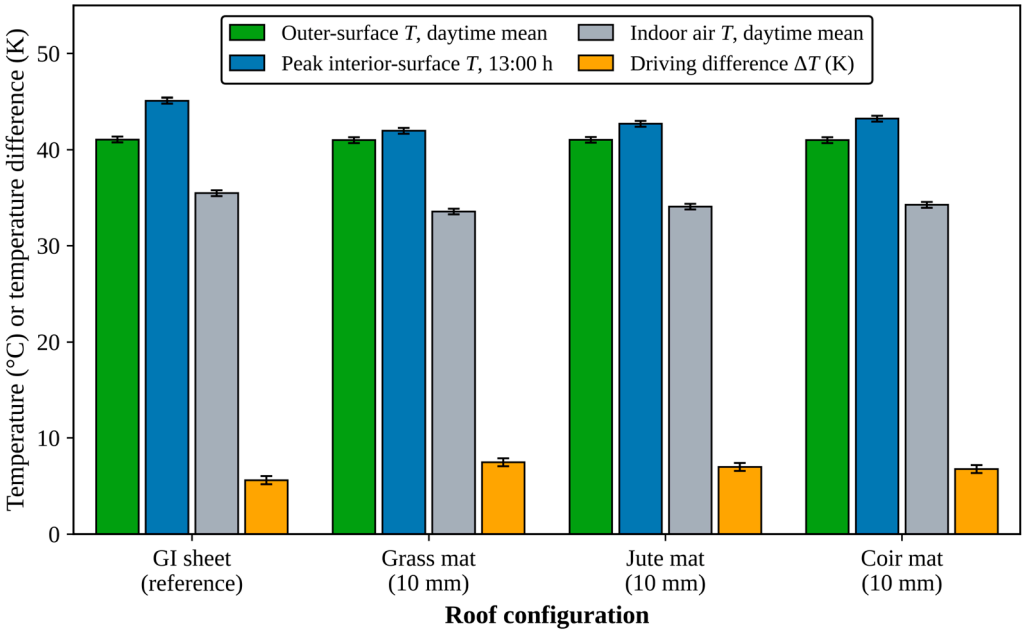


Figure 4. Measured temperatures of the roof configurations. Error bars show ±0.3 °C for single readings and ±0.42 K for differences.

3.2. Diurnal Thermal Response

Figure 5 presents the interior-surface temperature of each test labor shed, together with the indoor air temperature of each shed and the outdoor air temperature, over the representative day. Three regimes are evident. Outdoor air temperature ranged from 30.0 °C at 06:00 h to 39.0 °C at 14:00 h. Under low external loading between 00:00 and 06:00 h, all sheds converged toward 29 °C, with an interior-surface spread of 0.33 K at 05:00 h. Linings have little effect when the driving difference is small. The profiles diverged with solar heating. The largest difference occurred at 13:00 h, when the reference reached 45.10 °C and the grass shed reached 41.97 °C. The reference shed's indoor air peaked at 39.80 °C at 13:00 h, 0.8 K above the outdoor maximum.

In all sheds, the highest hourly reading occurred at 13:00 h; hourly logging cannot show whether the true peaks differed by less than 1 h. The single-capacity time constants in Table 5 are 0.11 h for the bare sheet and 0.44 to 0.57 h for the single mats. Because a time constant does not define a periodic phase lag, Table 5 also reports the ISO 13786 periodic response. The calculated time shifts are 1.0 min for the bare sheet and 3.5 to 5.4 min for the single mats. All calculated shifts are shorter than the 60 min sampling interval, so hourly data can neither confirm nor rule them out. The data therefore support a sub-hourly shift and do not show an unchanged phase. Resolving the shift requires sampling at 5 min intervals or shorter. Assemblies that achieve time lags near 9 h rely on thick, massive layers rather than thin fiber mats [13].

Table 5. Dynamic thermal characteristics of the roof configurations.

Configuration	Peak $T_{s,in}$ (°C)	Minimum $T_{s,in}$ (°C)	Diurnal Swing (K)	Relative Attenuation, f	κ (kJ m^{-2} K^{-1})	τ (h)	f_d (ISO 13786)	Δt_φ (min)
GI sheet (reference)	45.10	29.02	16.08	1.000	1.92	0.11	1.000	1.0
Grass mat	41.97	28.69	13.28	0.826	4.76	0.57	1.000	5.4
Jute mat	42.70	28.98	13.72	0.853	3.42	0.44	1.000	3.5
Coir mat	43.23	28.99	14.24	0.885	3.93	0.45	1.000	4.0

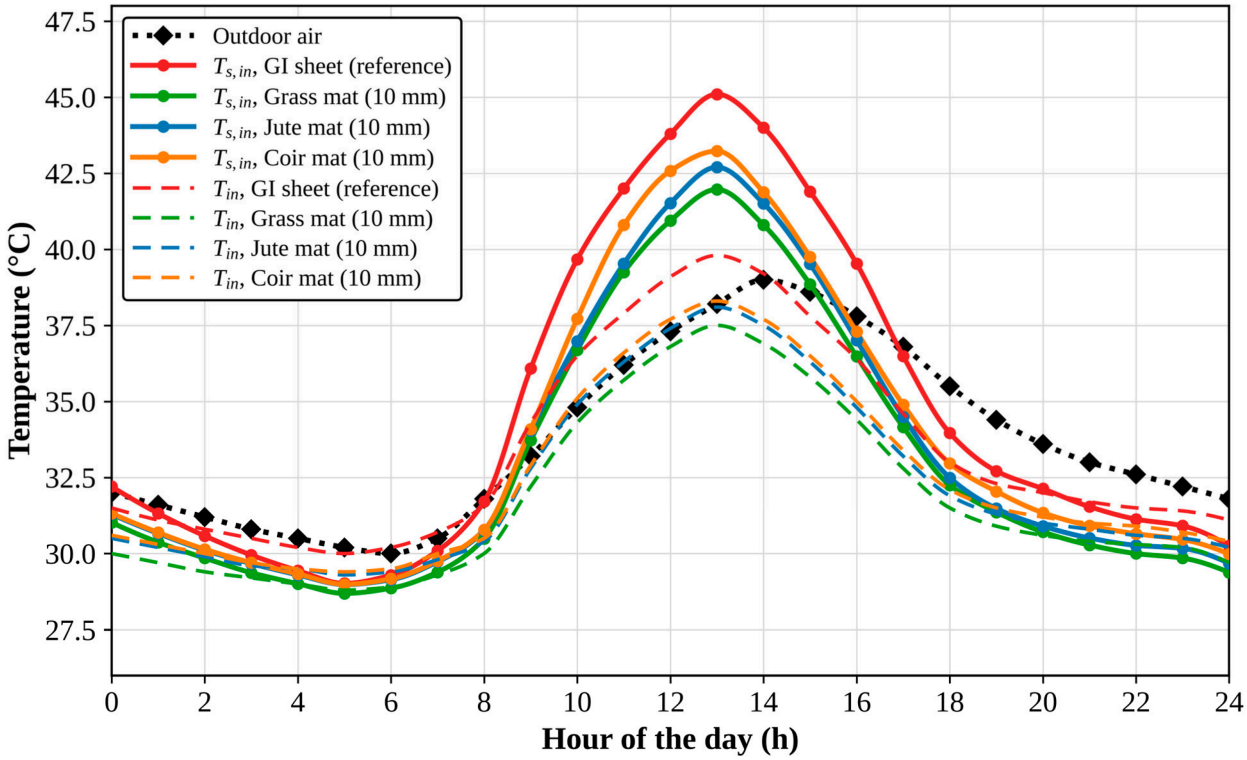


Figure 5. Diurnal profiles of interior-surface temperature and indoor air temperature in the GI reference and the three lined labor sheds, with outdoor air temperature, on the representative day (11 May 2026).

The linings reduced the measured amplitude through attenuation, and no phase shift was observed at the hourly time interval. The attenuation factors for grass, jute, and coir were 0.826, 0.853, and 0.885, respectively, compared with the reference swing of 16.08 K. The grass mat reduced the diurnal swing at the inside surface by 17.4%. The areal heat capacity of the grass assembly (4.76 kJ m^{-2} K^{-1}) is small in absolute terms, although it exceeds that of the bare sheet (1.92 kJ m^{-2} K^{-1}). The improvement is therefore largely due to added resistance, not to storage. This reading is supported by the calculated decrement factors of 1.000, as the periodic transmittance is almost the same as the steady U-value. All profiles decreased after the afternoon maximum and then merged again to 29.86–30.91 °C at 23:00 h. The linings reduced the measured amplitude (attenuation), with no phase shift at the hourly time interval. The diurnal reduction in swing for grass, jute, and coir was 17.4%, 14.7%, and 11.5%, respectively, compared with the reference swing of 16.08 K. The absolute value of the areal heat capacity of the grass assembly (4.76 kJ m^{-2} K^{-1}) is small, but is greater than that of the bare sheet (1.92 kJ m^{-2} K^{-1}). Much of the improvement is due to the added resistance rather than to storage. The calculated decrement factors are 1.000, supporting this reading. All profiles dropped following the afternoon maximum and then converged again to 29.86 to 30.91 °C at 23:00 h.

3.3. Calculated Steady-State Performance

The steady-state performance is calculated and shown in Table 6; the resistance build-up, U-value, and reduction indices are shown in Figures 6–8, respectively. The calculated total resistance of the bare GI assembly is 0.210 m^2 K W^{-1}, with the surface films providing nearly all of this resistance. The resulting U-value is 4.76 W m^{-2} K^{-1}. A daytime heat flux of 32.90 W m^{-2} (651.3 W over the 19.8 m2 roof) is estimated. When the mat is 10 mm thick, the calculated total resistance is between 0.410 and 0.460 m^2 K W^{-1}. The U-value falls to 2.44 W m^{-2} K^{-1} for coir, 2.31 W m^{-2} K^{-1} for grass, and 2.17 W m^{-2} K^{-1} for jute. These are

reductions of 48.78%, 51.41%, and 54.35%, respectively. The estimated heat flux falls to 18.23, 19.00, and 16.59 W m^{-2}. The estimated heat-transfer rate is 275.2 to 322.8 W lower than the reference. The ordering of the U-values is based only on the measured conductivities, while the order of the fluxes also accounts for the highest measured driving difference in the grass shed.

Table 6. Calculated and estimated steady-state thermal performance of the roof configurations.

Configuration	R_{total} (m^2 K W^{-1})	U (W m^{-2} K^{-1})	U Reduction (%)	q (W m^{-2})	HGR (%)	Q (W)	ΔQ vs. Reference (W)
GI sheet (reference)	0.210	4.76	0.00	32.90	0.00	651.3	0.0
Grass mat (10 mm)	0.432	2.31	51.41	19.00	42.26	376.1	275.2
Jute mat (10 mm)	0.460	2.17	54.35	16.59	49.56	328.5	322.8
Coir mat (10 mm)	0.410	2.44	48.78	18.23	44.57	361.0	290.3

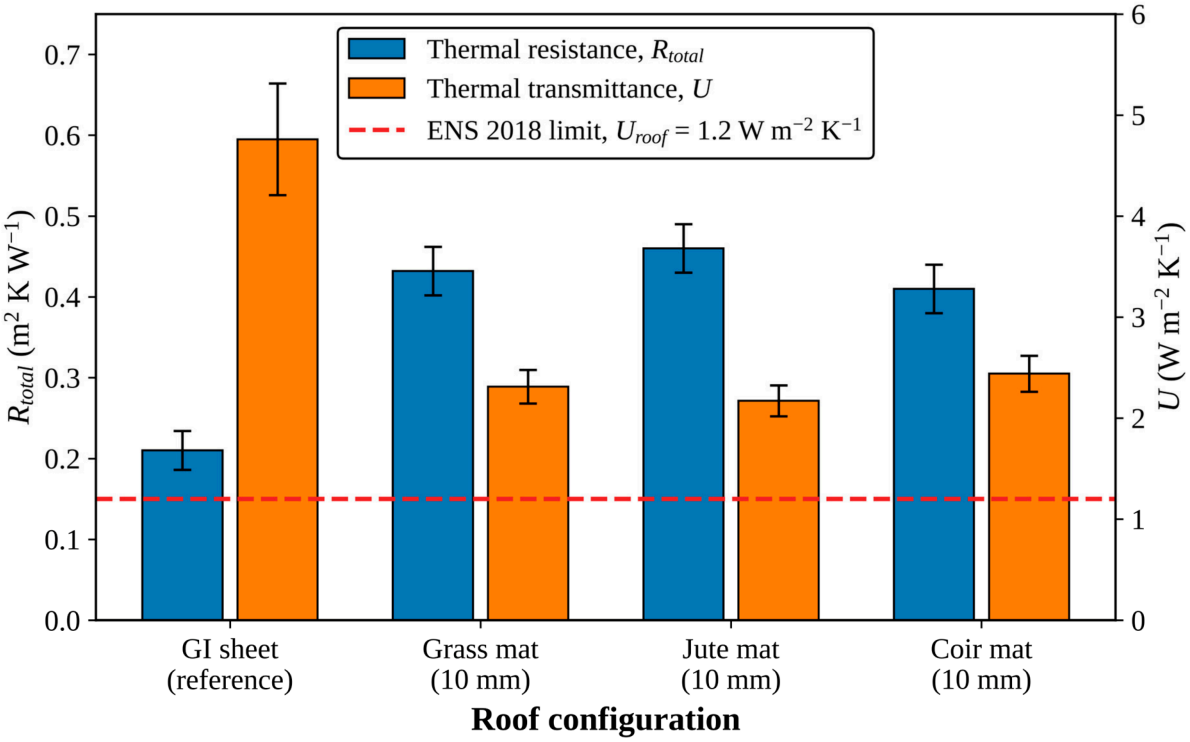


Figure 6. Calculated thermal resistance and U-value of the roof configurations, showing the ENS roof criterion of 1.2 W m^{-2} K^{-1}.

The uncertainties of the total resistance are ±0.024 m^2 K W^{-1} for the reference and ±0.030 m^2 K W^{-1} for the lined assemblies. These relative uncertainties in U-value were 11.62% for the bare sheet and 7.07% to 7.28% for the single mats. As resistance increases, the fixed-film and contact terms decrease, and the relative uncertainty decreases. The 0.27 W m^{-2} K^{-1} range of the single-mat U-values is approximately the same as these limits, and the calculated U-values do not distinguish the mats.

Equation (4) neglects heat storage. From Equations (14) and (15), the stored energy is 30.9 kJ m^{-2} for the bare sheet and 46.9 to 63.2 kJ m^{-2} for the single mats. These values equal 2.2% and 6.5% to 7.7% of the estimated daytime conducted energy, or mean fluxes of 0.71 and 1.09 to 1.46 W m^{-2}. Some stored heat is released before 18:00 h, so the net error over the daytime window is likely smaller. The storage share of up to about 8% is comparable to the 7.07% to 7.28% propagated U-value uncertainty of the single mats.

Validation against heat-flow measurements or a transient model calibrated to sub-hourly data remains necessary.

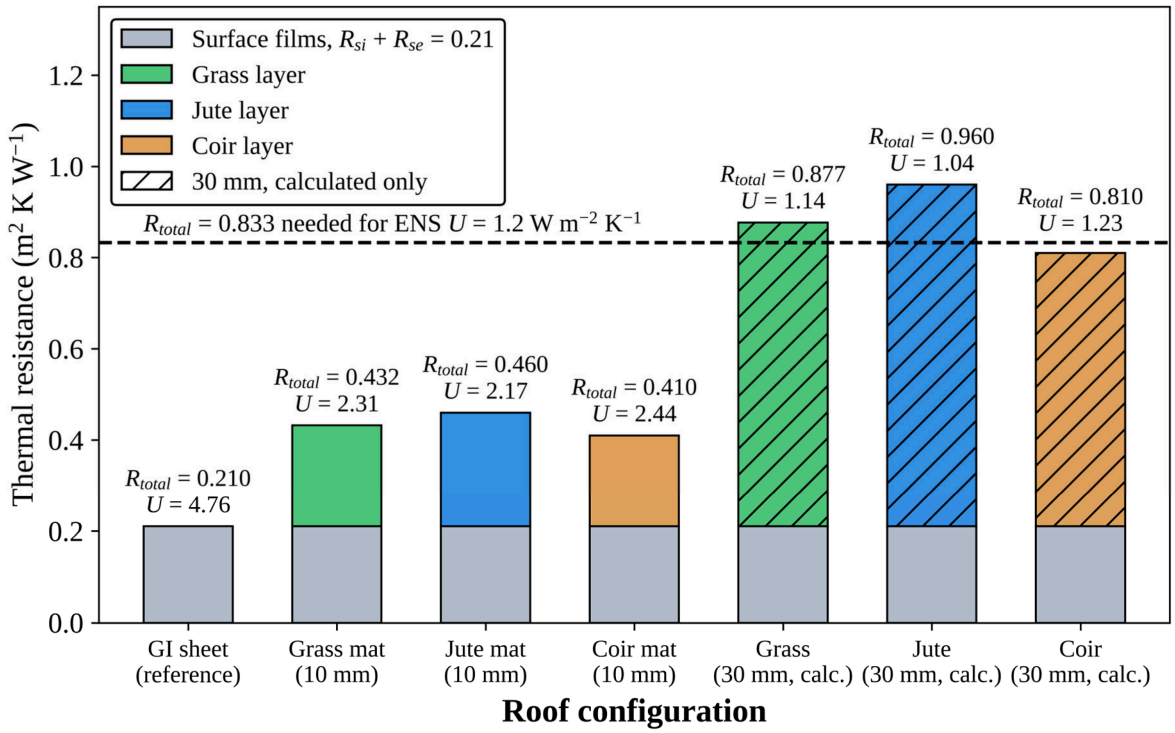


Figure 7. Layer-by-layer build-up of calculated thermal resistance for the tested 10 mm linings and for calculated 30 mm single-material linings, with the total resistance needed to meet the ENS roof criterion.

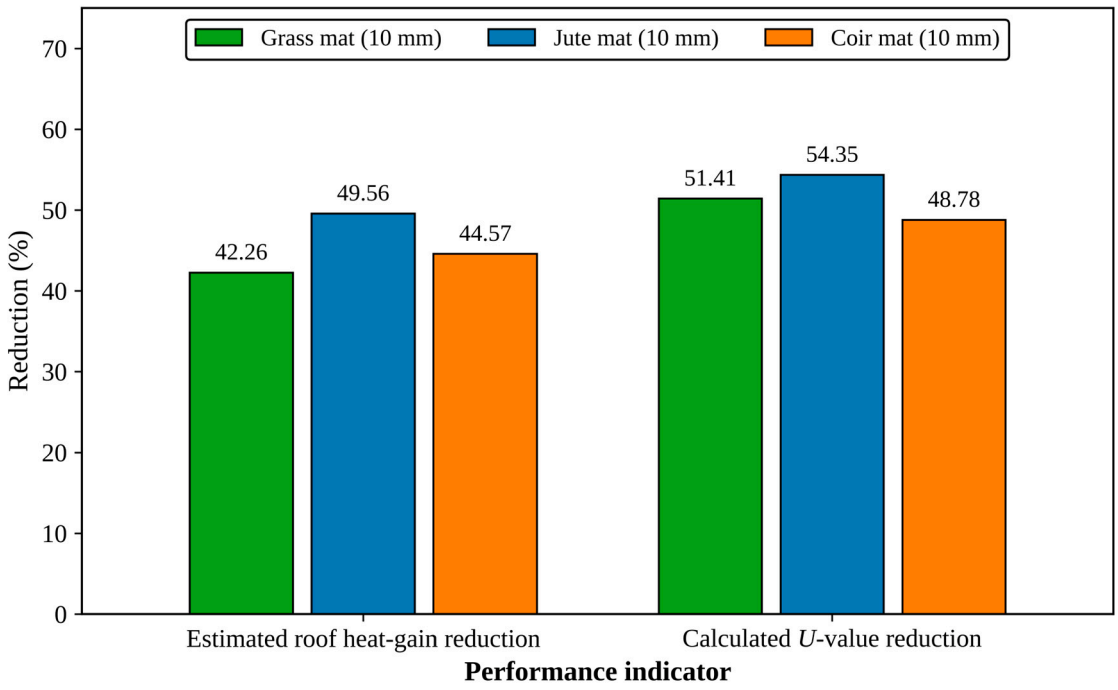


Figure 8. Estimated heat-gain reduction and calculated U-value reduction relative to the unlined GI reference.

3.4. Comparison of the Single-Material Linings

At the tested 10 mm thickness, the measured and calculated evidence points in different directions. The measured peak interior-surface reductions span 1.26 K and the daytime-mean indoor air reductions span 0.70 K; both exceed the ±0.42 K resolution and both rank grass first. The calculated U-values, by contrast, span only 0.27 W m^{-2} K^{-1}, comparable to the 7% propagated uncertainty on each value, and rank jute first. Grass has the highest areal mass (1.35 kg m^{-2}) and areal heat capacity of the three mats, so its field advantage may partly reflect installed contact, compaction, or cavity conditions that the series model does not capture. The position of each shed in the row may also contribute, because each treatment occupied one shed. The field ranking was held on each of the 21 measured days, but a formal comparison requires replicated sheds with rotated treatments (longitudinal studies).

This small difference in calculation is acceptable for fiber insulation. The reported conductivity of the straw-based panels varied by a factor of 3 across measurement methods [11], much more than the variation among the three mats. The thermal conductivity of natural fiber-reinforced composite boards is influenced by fiber lumen size, the ratio of fiber-to-matrix conductivity, fiber volume, and the board's density and porosity, and indirectly by fiber pre-treatment, the manufacturing process, and environmental conditions [33]. Such changes may occur during installation if compaction shifts a particular mat within the measured property width. The thermal conductivity of 25 flax fiber waste panels ranged from 0.029–0.325 W m^{-1} K^{-1} and showed a power-law dependence on bulk density [34].

The measured advantage of grass exceeded the measurement resolution at 10 mm thickness, while the calculated differences were minor. Other factors that can influence material choice include local availability, durability, and ease of installation. Grass mats are commonly used for matting and shading in Tamil Nadu. Coir fiber is also a byproduct of coconut processing and is widely used in bio-composites [35].

3.5. Thickness Required to Meet the Roof Criterion

The U-value in the ENS roof criterion depends on lining thickness, not fiber type. The 10 mm mat thickness is inadequate to satisfy the U-value requirement specified in the ENS roof criterion. In the series model, a U-value of 1.2 W m^{-2} K^{-1} requires a total resistance of 0.833 m^2 K W^{-1}. With the surface films supplying 0.210 m^2 K W^{-1}, the mat must add 0.623 m^2 K W^{-1}. This corresponds to 24.9 mm of jute, 28.0 mm of grass, or 31.2 mm of coir (Figure 7). At 30 mm, the calculated U-values would be 1.04 W m^{-2} K^{-1} for jute, 1.14 W m^{-2} K^{-1} for grass, and 1.23 W m^{-2} K^{-1} for coir. The gain is not directly proportional to the thickness, as the U-value is inversely proportional to total resistance. Each additional layer therefore yields a diminishing return. Thickness sensitivity analysis has been used on the same principle to optimize the hygrothermal performance of cob walls [36].

3.6. Reconciling Roof Heat-Transfer Reduction with the Indoor Response

The calculated roof U-values decreased by 48.78–54.35%, and the indoor air temperature during the day decreased by 1.22–1.92 K. Table 7 and Figure 9 provide a partial explanation: envelope decomposition. The uninsulated GI walls had a measured area of 44.5 m^2, and the calculated U-value was 5.88 W m^{-2} K^{-1}, which gives a wall conductance of 261.7 W K^{-1}. The bare roof contributes 94.3 W K^{-1} over 19.8 m^2. Therefore, the roof accounts for 26.5% of the conductive envelope conductance, and the walls account for 73.5%.

Table 7. Calculated labor shed envelope conductance.

Configuration	Roof *UA* (W K^{-1})	Wall *UA* (W K^{-1})	Envelope *UA* (W K^{-1})	Roof Share (%)	Envelope Reduction (%)
GI sheet (reference)	94.3	261.7	356.0	26.5	0.0
Grass mat (10 mm)	45.8	261.7	307.6	14.9	13.6
Jute mat (10 mm)	43.0	261.7	304.8	14.1	14.4
Coir mat (10 mm)	48.3	261.7	310.0	15.6	12.9
Jute mat on roof and walls (10 mm, scenario)	43.0	105.9	149.0	28.9	58.1

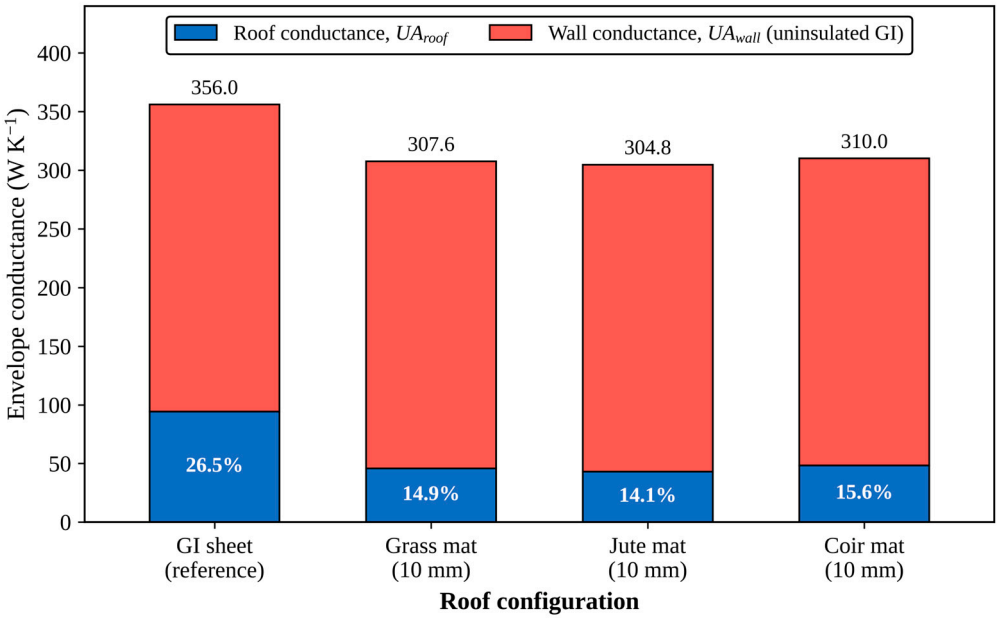


Figure 9. Decomposition of calculated envelope conductance into roof and wall contributions.

This share only refers to conductive conductance and not the actual roof share of solar heat gain. Each wall will have a different surface temperature depending on orientation, which was not measured; the near-horizontal roof will receive its highest solar radiation at midday. Other factors contribute to the indoor heat balance, such as infiltration and ventilation, floor exchange, and internal gains. The labor sheds were unoccupied during the day, and no electrical or mechanical equipment operated in them during monitoring. The thermal conductance shares therefore show why a roof-only measure has limited leverage on indoor air temperature, but they do not quantify the roof contribution to indoor cooling. That quantification requires measured wall surface temperatures, air-change rates, and a zone heat balance.

Lining the roof shifts this balance, but the walls remain the dominant path. The single mats reduce envelope conductance from 356.0 W K^{-1} to 304.8 to 310.0 W K^{-1} (12.9% to 14.4%) and lower the roof share to 14.1% to 15.6%. Within the conductive network, a roof-only intervention cannot reduce envelope conductance by more than 26.5%, no matter how effective the lining. This is the main practical limitation of a roof-only retrofit. The measured 1.22 to 1.92 K indoor reduction is consistent with, but not proven by, this bound.

Air temperature also understates the thermal burden. Even in the grass shed, the lining surface reached 41.97 °C at peak, while the daytime-mean indoor air temperature was 33.55 °C. The hot ceiling and the surrounding metal walls exchange long-wave radiation with occupants independently of air temperature. Operative temperature (Equation (10))

is therefore the more appropriate comfort metric. Air temperature alone may understate both the problem and the benefit of radiant-surface interventions in lightweight labor sheds.

A first-order conductance scenario suggests treating the walls. Applying the same 10 mm jute mat to the walls, with an internal surface resistance of 0.13 m^2 K W^{-1} for horizontal heat flow [26], would lower the wall U-value from 5.88 to 2.38 W m^{-2} K^{-1} and the wall conductance from 261.7 to 105.9 W K^{-1}. Combined with the jute-lined roof, envelope conductance would fall to 149.0 W K^{-1}, a 58.1% reduction relative to the bare labor shed. This is about four times the roof-only reduction. The scenario assumes identical installed properties and contact conditions, the same U-value behavior on vertical surfaces, no thermal bridging, no moisture effect, and no geometric or installation changes. It is a sensitivity estimate, not a measured result. Insulation placement, material and thickness, and external surface absorptivity have been assessed as determinants of roof heat gain and loss for buildings in India [37].

3.7. Code and Comfort Benchmarking

ENS 2018 specifies a maximum roof U-value of 1.2 W m^{-2} K^{-1} for residential buildings in all climate zones of India (Section 3.3, Thermal Transmittance of Roof, p. 7) [38]. The code applies to residential buildings above a plot-area threshold. Its legal applicability to temporary worker labor sheds is not established, so it is used here only as a numerical benchmark. The bare GI roof (4.76 W m^{-2} K^{-1}) is 3.97 times the criterion. The single 10 mm mats, at 2.17 to 2.44 W m^{-2} K^{-1}, remain 81% to 103% above it. None of the tested linings meet the criterion, and Section 3.5 gives the required thickness.

The mean daily outdoor temperature from 1 to 21 May 2026 (Equation (19)) was 35.8 °C, and the mean from 1 to 10 May, the period preceding the representative day, was 35.9 °C. Both exceed the 31 °C applicability limit of IMAC, so the model was evaluated at that limit. The IMAC neutral temperature is then 29.57 °C, and the upper limits of the 90% and 80% bands are 31.97 °C and 33.67 °C. Figure 10 compares the measured daytime-mean indoor air temperatures and the estimated operative temperatures with these bands. The bare labor shed (35.47 °C) exceeds the 80% limit by 1.80 K. Grass falls 0.12 K inside that limit, whereas jute and coir lie 0.39 and 0.58 K above it, margins comparable to the measurement uncertainty. The estimated daytime-mean operative temperatures were 0.15 to 0.18 K above the air temperatures (35.65 °C for the reference and 33.70 to 34.41 °C for the mats). Over the 24 h of 11 May, the estimated operative temperature exceeded the 80% limit for 9 h in the reference and 7 h in each lined shed. Because the wall surfaces were assigned the air temperature, these operative values are lower bounds. IMAC is defined based on operative temperature, so the comparison remains indicative.

On this indicative basis, roof lining alone moves the labor sheds from beyond the 80% band toward its margin, but not into the 90% band. No comfort acceptability is claimed without validated operative temperature. Comparison with published field values follows in Section 3.9, after the differences in design and outcome definition are set out.

3.8. Mean Response over the 21-Day Monitoring Period

Table 8 and Figure 11 summarize the 21 measured days. Daily outdoor maxima ranged from 37.6 to 43.4 °C and minima from 29.2 to 32.7 °C, with means of 40.9 and 30.8 °C. The 24 h mean indoor air temperature of the reference shed ranged from 32.30 to 36.37 °C and averaged 34.43 °C, only 0.31 K below the mean outdoor air temperature. The lined sheds averaged 32.79 °C for grass, 33.28 °C for jute, and 33.44 °C for coir.

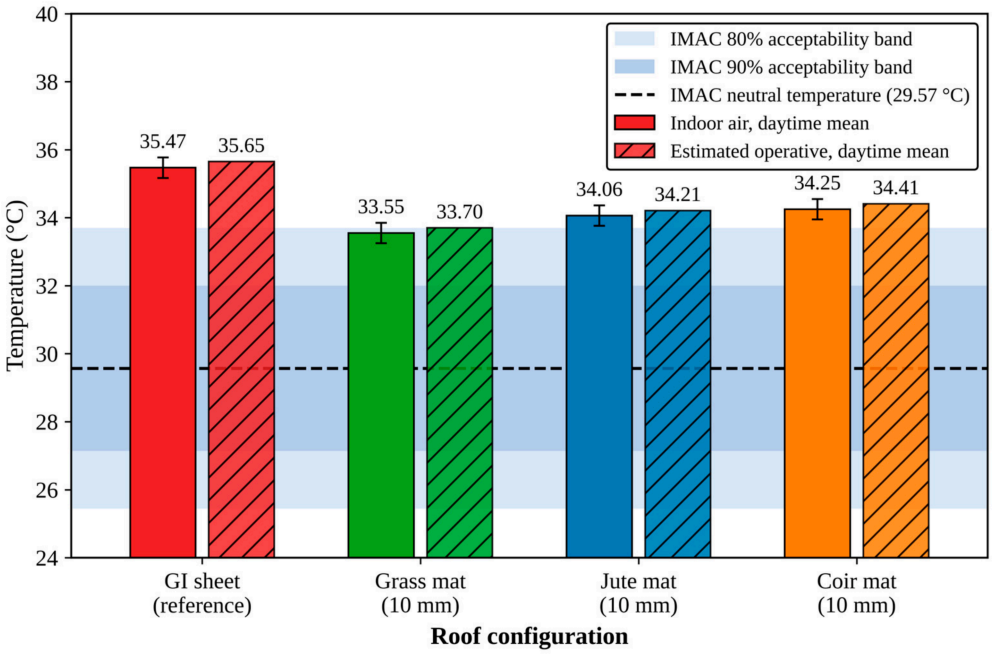


Figure 10. Measured daytime-mean indoor air temperature and estimated daytime-mean operative temperature on 11 May 2026 against the IMAC acceptability bands.

Table 8. Mean response of the roof configurations (each mat with 10 mm thickness) from 1 to 21 May 2026 (mean, with the range of daily values in parentheses).

Configuration	Mean T_{in}, 24 h (°C)	Range of Daily-Mean T_{in} (°C)	Outdoor Minus Indoor Air, 24 h (K)	Daytime-Mean T_{in} Reduction (K)	Peak $T_{s,in}$ Reduction (K)	Overheating Hours (h day^{-1})
GI sheet (reference)	34.43	32.30–36.37	0.31 (0.26–0.37)	–	–	10.6 (7–19)
Grass mat	32.79	30.74–34.73	1.95 (1.82–2.11)	1.90 (1.78–2.04)	3.04 (2.57–3.59)	7.9 (5–11)
Jute mat	33.28	31.23–35.22	1.47 (1.33–1.62)	1.38 (1.27–1.52)	2.32 (1.93–2.78)	8.6 (5–13)
Coir mat	33.44	31.38–35.38	1.30 (1.18–1.44)	1.20 (1.10–1.32)	1.81 (1.50–2.17)	8.6 (5–14)

Over the period, the measured daytime-mean indoor air reduction relative to the reference averaged 1.90 K for grass (range 1.78 to 2.04 K), 1.38 K for jute (1.27 to 1.52 K), and 1.20 K for coir (1.10 to 1.32 K). The measured peak interior-surface reduction averaged 3.04, 2.32, and 1.81 K. The daily ranges of the three mats do not overlap, so the order grass, jute, and coir held on every day. The operative temperature estimated from the measured temperatures exceeded the IMAC 80% limit for 10.6 h day^{-1} in the reference and for 7.9 to 8.6 h day^{-1} in the lined sheds. The 21-day mean reductions are within 0.03 K of the 11 May values, confirming that the representative day is typical of the period.

Day-to-day variation followed the outdoor diurnal range. The largest reductions occurred on 16 May (range 12.2 K) and the smallest on 12 May (8.4 K). Because irradiance and wind speed were not logged, this dependence is reported as an observation rather than as a regression. Replicated sheds with logged irradiance are needed to quantify the weather sensitivity, confidence intervals, and any formal equivalence of the mats.

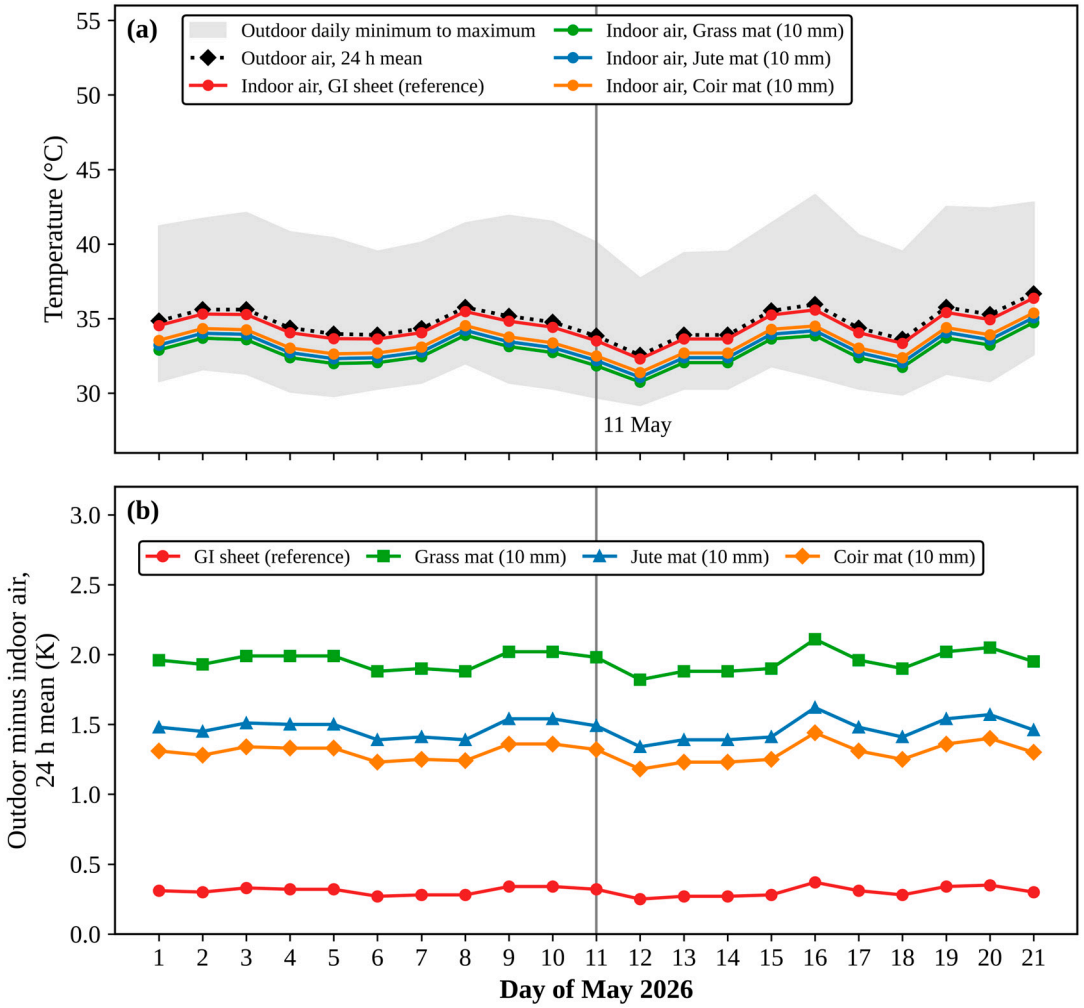


Figure 11. Measured daily response from 1 to 21 May 2026: (**a**) Outdoor daily range and 24 h mean, and 24 h mean indoor air temperature of each test labor shed; (**b**) Mean difference between outdoor and indoor air temperatures over 24 h. The vertical line indicates the reference day with a detailed analysis.

3.9. Comparison with Published Field and Simulation Studies

Table 9 compares the present design with recent cost-effective roof and lining studies. The studies differ in climate, building type, lining thickness, monitoring duration, replication, and whether they measured or estimated the outcome. Outcome definitions differ as much as designs. Ang et al. [17] report a mean indoor effect over long minute-level records, whereas Wilby et al. [3] report separate day and night means from between-room contrasts that also differ in construction. Amankwaa et al. [2] reported overheating hours rather than a temperature difference. The present 1.22 to 1.92 K is a daytime mean (06:00 to 18:00 h) of a paired shed contrast on one clear-sky day, excluding the cooler night; the corresponding measured 24 h means over the 21 days were 0.99 to 1.64 K. A daytime-only mean on a clear day will exceed a full-day mean over mixed weather. These values should therefore be compared with the 1.24 K for radiant foils only qualitatively, as both indicate indoor reductions of about 1 to 2 K from cost-effective roof-side measures. The 3.5 °C simulated reduction for straw insulation [18] applies to the peak rather than the mean and to a full envelope rather than a roof-only lining. The cool-ventilated roof result [39] reduces absorbed solar flux at the source, a mechanism distinct from lining.

Table 9. Comparison of experimental design, outcome definition, and reported effect with published studies. Tabulated values are general reference values quoted in the source, not measurements of the tested lining.

Study	Location and Climate	Building and Lining	Design, Duration, and Replication	Basis	Outcome and Reported Effect
Amankwaa et al. [2]	Accra, Ghana; tropical	Classrooms; plywood (12 mm thick, λ = 0.07–0.15 W m^{-1} K^{-1}) ceiling under metal roof	Field; 16 classrooms; 389 days; between-room	Measured	Overheating hours halved relative to bare metal roof
Wilby et al. [3]	Accra and Tamale, Ghana	Living rooms in eight low-income communities; ceiling insulation-plywood, plastic sheeting	Field; 47 rooms; between-room	Measured	Day mean 6.9 °C cooler; night mean 1.4 °C warmer
Ferencz et al. [15]	Bácsalmás, Hungary; temperate continental	Container houses; internal phase change material–gypsum plaster lining (25 mm thick)	Field; 105 days; one reference and one treated house	Measured	Timing of heat transfer reshaped; net exchange reduced
Ang et al. [17]	Bihar, India	Informal dwellings in two communities; radiant foil and Mylar blanket	Field; over 2 million minute-level observations	Measured	Indoor reduction of 1.24 °C (foil) and 0.97 °C (Mylar)
Sabapathy and Gedupudi [18]	Five Indian climate zones	Naturally ventilated 3 m × 3 m × 2.5 m room; straw envelope insulation	Computational fluid dynamics simulation; representative days	Simulated	Peak indoor air reduction up to 3.5 °C
Athmani et al. [39]	Biskra, Algeria; hot dry	Test cells; cool-ventilated roof	Field; 5 summer days	Measured	Average indoor temperature reduced by 4.95 °C
Sigikumar et al. [40]	India (8.91° N, 76.63° E); tropical	Two test cubicles; dry coir mat laid over the roof slab	Field; one treated and one reference cubicle; 24 h	Measured	Heat transfer through the roof reduced by 38.43%
Sigi Kumar et al. [41]	India; tropical	Two test cubicles; dry and wet coir mat on one wall	Field; treated wall against a reference wall; 24 h	Measured	Heat mitigation potential of 41.45% (dry mat) and 36.3% (wet mat)
Cigarruista Solís et al. [42]	Chitré, Panama; tropical savanna	Two test chambers with galvanized steel sheet roof; rice husk roof-insulation panels (15 mm thick, λ = 0.073 W m^{-1} K^{-1})	Field; one treated and one reference chamber; April and May 2021	Measured	Inward roof heat flux up to 28.18 W m^{-2} without panels; rarely observed with panels
Vimalraj et al. [43]	Sivakasi, India; tropical	Two test huts; coconut-leaf thatch roof against terracotta tiles	Field; one treated and one control hut; one sunny day	Measured	Interior at 33.36 °C against 34.51 °C (1.15 °C lower)
Present study	Chennai, India; warm-humid	19.8 m^2 GI labor sheds; grass, jute, and coir mats (10 mm thick, λ = 0.04–0.05 W m^{-1} K^{-1})	Field; four simultaneous labor sheds, one per treatment; hourly records for 21 days (1 to 21 May 2026); 24 h analysis on 11 May	Measured T; calculated U; estimated q	Daytime-mean indoor air reduction of 1.22 to 1.92 K on 11 May; measured 21-day 24 h mean reduction of 0.99 to 1.64 K

Four field studies of natural-fiber roof and wall layers in tropical climates are the closest comparators. A dry coir mat laid over a roof slab reduced heat transfer through the roof by 38.43% relative to a bare roof [40], and a dry coir mat on a wall showed a 24 h heat mitigation potential of 41.45% [41]. These reductions are of the same order as the estimated heat-gain reduction of 42.26% to 49.56% obtained here, although those mats covered the outer side of masonry elements rather than the underside of a metal sheet. Under a galvanized steel roof in Panama, an inward roof heat flux of up to 28.18 W m^{-2} occurred in the uninsulated chamber and was rarely observed in the chamber with 15 mm rice husk panels (0.073 W m^{-1} K^{-1} conductivity) [42]. The estimated flux for the bare GI roof in the present study, 32.90 W m^{-2}, indicates comparable roof loading. In a coconut-leaf thatched hut in southern India, the interior was 1.15 °C cooler than in a tiled control hut [43], close to the 1.22 to 1.92 K daytime-mean reductions measured here. None of these studies compared grass, jute, and coir under one roof, and field evidence for grass and jute mats beneath metal roofs in hot-humid climates remains scarce. Only the rice husk panel study reports both lining thickness and measured conductivity, limiting direct material comparison. The present study pairs measured lining conductivity with a simultaneous contrast of three natural-fiber linings and a bare reference.

3.10. Moisture, Durability, and Fire Considerations

Durability under hygrothermal conditions affects measured performance over time. Bio-based insulation is a type of insulation whose porous structure continuously changes its hygric and thermal properties through water vapor sorption and desorption [44]. This study did not measure moisture content. Therefore, the reported performance reflects dry conditions before the monsoon and may overestimate performance under humid monsoon conditions. Another potential hazard in a coastal tropical setting is biological decay. None of the cellulose-insulated walls monitored for 1 year and 9 months had mold behind the wall, while all four hemp-fiber-insulated walls showed mold growth with Mycometer surface values over 400 [45]. Those walls are not like a metal roof in terms of construction and climate. The results show that mold risk depends not only on bulk moisture content but also on the water level at fiber interfaces.

The three measures for labor sheds are as follows. First, keep rainwater away from sheet laps and eaves by keeping the lining away. Second, fiber surface modification can enhance durability and moisture tolerance [46]. Third, the degradation rate of plant fibers in service depends on their composition and morphology, so inspection and planned replacement seem appropriate [47].

One significant drawback is fire performance. Lignocellulosic mats can burn, and on the underside of a roof, they would be subjected to a compartment fire. Bio-based construction materials are flammable, and reducing their fire risk is a recognized concern [48]. Untreated mats should not therefore be used in occupied buildings. The untreated material tested herein should not be deployed, as deployment should await a suitable fire assessment, such as a reaction-to-fire classification of the treated mat as installed. This study did not test moisture sensitivity, fire performance, service life, installed cost, or environmental impact. Each could alter the practical ranking of the linings, and none of them can be inferred from the thermal results.

3.11. Implications and Candidate Retrofit Sequence

The results suggest a candidate retrofit sequence, not an established optimum. The sequence ranks measures by calculated conductive leverage only. The first stage is a bio-based under-roof lining of about 25 to 31 mm, the calculated thickness needed to meet the ENS numerical roof criterion, subject to the measurements planned for May 2027. The

tested mats reduce the estimated roof heat transfer rate by 275.2 to 322.8 W over 19.8 m^2 at 10 mm thickness. The second stage is lining the metal walls, which account for 73.5% of the calculated envelope conductance. The conductance scenario also implies a 58.1% reduction in envelope conductance for the same 10 mm jute mat, considering both roof and wall, and it needs field verification. The third stage is surface treatment of the external surface to lower absorbed solar radiation. Each stage requires fire assessment of treated mats, moisture and service-life testing, and installed-cost data.

Lining is not a substitute for reflective and ventilated measures. A lining resists the transmission of absorbed solar flux, whereas a reflective surface reduces the absorbed flux at the source. Combining the two addresses both stages of the roof heat balance. For building roofs in Mexico, an insulated white roof had up to 6.4 times less daily heat gain than a non-insulated gray roof [49]. This combination suits new transitional labor sheds.

3.12. Carbon and Stakeholder Implications

The monitored labor sheds are naturally ventilated; therefore, the benefit is thermal, not energy-saving. A carbon benefit arises only where the heat would otherwise be removed mechanically, or where the linings displace insulation with a higher embodied impact. For example, the 275.2 to 322.8 W reduction in daytime roof heat-transfer rate equals 3.3 to 3.9 kWh of heat over a 12 h day. With an assumed air-conditioner coefficient of performance of 3.0, the avoided electricity would be 1.1 to 1.3 kWh per day. This corresponds to about 0.80 to 0.94 kg CO_2 per unit per day at the 2023–24 weighted average emission factor of the Indian grid, 0.727 t CO_2 MWh^{-1}, which includes renewable sources (Table S, p. 2 of [50]). These are scenario-based rather than measured savings, because they rest on an estimated heat flux, an assumed coefficient of performance, and continuous daytime cooling. Plant-based mats are also biodegradable and recyclable [6], although no life cycle assessment was performed here.

Stakeholder benefits vary across GI-sheds. Workers gain a ceiling surface that is about 2 to 3 K cooler at peak heat and slightly lower indoor air temperatures during the day. Contractors and site owners gain a retrofit that is simple to install, leaves the frame unchanged, and uses locally traded materials to slightly reduce indoor temperatures. Local grass, jute, and coir producers gain an additional market. Regulators and welfare agencies gain field evidence that a 10 mm roof lining roughly halves the calculated roof U-value yet still fails the ENS roof criterion and leaves most of the envelope conductance unchanged, supporting the inclusion of wall treatment in minimum standards for labor sheds. Before these benefits can be realized, gaps in fire, moisture, durability, and cost must be addressed, along with packing methods for such natural fibers to ensure thermal comfort and safety.

4. Limitations and Future Work

4.1. Limitations of the Study

The findings of this study are limited by the following constraints, which bound how far the results can be generalized.

- The field study was conducted at a single site using one row of labor sheds during one season. Only one labor shed was tested per treatment, and treatments were not rotated. Therefore, shed location, wall exposure, and local ventilation conditions may also influence the effects of the lining materials. Hence, the findings should be considered a field case study rather than a general performance rating applicable to all labor sheds.
- Roof heat flux was estimated, not measured, so the calculated U-values are not independently verified. Equation (4) neglects storage, which may bias the single-mat estimates by up to about 8%.

- Only linings up to 10 mm have been analyzed. It was not possible to build and monitor liners thicker than 10 mm in May 2026; therefore, this study calculated the required thickness based on the ENS criterion.
- Only one pre-monsoon season (1–21 May) 2026 was observed during the shed-level temperature measurements. No information is provided on its performance during the monsoon season, post-monsoon, or at low occupancy.
- Only underneath roof insulation was investigated. The side partitions connect to other sheds, and no study was conducted on the insulation of any exposed front or back walls.
- The properties of mats were determined on laboratory specimens. Thickness and compaction may differ during installation, which may lead to variations in effective conductivity within the measurement uncertainty range.
- Solar irradiance and wind speed were not measured. This is not a bias when comparing one shed to another, but it prevents normalization for irradiance and limits the weather-sensitivity analysis to a single observation.
- Air and heat exchange between the test sheds and the intervening empty sheds, through the partitions and the gaps in the corrugated sheet, may have made the measured differences smaller or larger; their direction and size were not measured, and air-change rates were not logged.
- The corrugated sheet left air cavities between the sheet and the mats. These cavities, and any airflow through them, were not included in the calculated resistances or measured.
- Moisture content and interfacial relative humidity were not logged, so the hygrothermal discussion rests on published evidence.
- MRT and operative temperature were estimated from surface temperatures and a calculated ceiling angle factor, with the walls assigned the air temperature, not measured with a globe thermometer. The IMAC comparison therefore remains indicative. The single-mat ranking rests on one shed per treatment rather than on a formal statistical test.
- Moisture sensitivity, fire performance, service life, installed cost, and environmental impact were not tested.

4.2. Future Scope

The major limitations listed above lead to the following future research directions.

- Replicated test labor sheds with rotated treatments, with more than one shed monitored, would separate out the effect of shed position, wall exposure, and local ventilation and would allow for confidence intervals and a formal equivalence analysis of the mats.
- Measuring the heat flux using in situ heat-flux measurement with heat-flow-meter plates at the ceiling, as described in ISO 9869-1 [24], would convert the estimated heat flux into a measured heat flux and confirm the U-values calculated above. Sampling every 5 min or less would enable calibration of a transient model, quantify the storage-related error, and resolve the sub-hourly time shift.
- Also, single-material grass, jute, and coir linings of 30 mm, along with intermediate thicknesses, will be monitored during the pre-monsoon period in May 2027 with the same protocol to test the calculated thickness effect and the requirement of 24.9 to 31.2 mm against field temperatures.
- Shed records made over time would give a seasonal record of the shed's performance, and a 12-month field test would follow the shed's performance and degradation within the mold-growing, occupied field.

- The combined roof and wall insulation, with the bio-fiber thickness sized for the comfort target, should be quantified. Monitoring a wall-lined labor shed and a roof-only labor shed in parallel would test the 58.1% envelope-conductance scenario.
- It would be interesting to see the change in performance across multiple compaction levels as measured in installed-state conductivity.
- If solar radiation is measured by a pyranometer and wind speed is measured by an anemometer, the reductions can be normalized for each case to the solar radiation, and the wind sensitivity of each lining can be quantified by regression.
- The air exchanges between treatments would be quantified by measuring the air-change rates with tracer gas, by sealing the spaces between the partitions and the corrugated sheet, and by logging the air temperature of the partition space of the empty sheds.
- The contribution could be quantified by measuring the air temperature in the cavity air space and the airflow between the corrugation and the mat, and by modeling the cavity as an enclosed air layer or a ventilated air layer according to ISO 6946 [26]. In addition to the under-roof insulation study, future work will evaluate layering bio-fiber materials above the GI sheet. Combining the inner lining with a reflective outer layer or incorporating a suitable phase-change material could help determine whether these measures provide additional thermal benefits and whether they reduce or delay the peak indoor temperature.
- Moisture content and interfacial relative humidity measurements during the pre-monsoon and monsoon seasons would reveal changes in the installed moisture content and heat capacity of each mat due to sorption.
- The wall temperatures assigned will be replaced by the temperature measured on the wall surface using a globe thermometer, which will then provide a validated operative temperature, and the comparison in the IMAC would shift from indicative to conclusive. It may also be possible to conduct a formal statistical test of the single-mat ranking with a replicated design.
- Prerequisites for any field recommendation are fire classification, moisture cycling, service-life monitoring, an installed-cost survey, and a life cycle assessment of treated mats.

5. Conclusions

This field study evaluated woven grass, jute, and coir mats as under-roof linings beneath the GI roofs of 19.8 m^2 temporary labor sheds in Chennai. The study combined measured material properties with continuous hourly records from four simultaneously monitored test labor sheds over 1 to 21 May 2026. The conclusions follow the three objectives.

- The 10 mm single-material linings substantially reduced the calculated roof heat transfer. Calculated total resistance rose from 0.210 m^2 K W^{-1} to 0.410–0.460 m^2 K W^{-1}, and the calculated U-value fell from 4.76 W m^{-2} K^{-1} to 2.17–2.44 W m^{-2} K^{-1}. The estimated HGR was in the range of 42.26% to 49.56% for grass to jute, and the estimated roof heat-transfer rate decreased by 275.2 to 322.8 W. The differences between the calculated mat values are within their propagated uncertainty.
- On the representative day, the peak interior-surface and daytime-mean indoor air temperature reductions ranged from 1.87 to 3.13 K and from 1.22 to 1.92 K, respectively, with grass showing the largest effect. These differences exceed the measurement resolution (±0.42 K) and are based on one shed per treatment; they are not consistent with the calculated U-values. The linings reduced the interior-surface swing by 11.5% to 17.4%, with calculated time shifts ranging from 3.5 min to 5.4 min, all less than one hour. Over the 21 measured days (1 to 21 May 2026), the 24 h mean indoor air temperature was 0.99 to 1.64 K below the reference; the estimated operative temperature

exceeded the IMAC 80% limit for 7.9 to 8.6 h day^{-1}, compared with 10.6 h day^{-1} for the bare roof.

- The uninsulated walls contribute 261.7 W K^{-1}, compared with 94.3 W K^{-1} for the bare roof, so the roof carries 26.5% of the calculated envelope thermal conductance. The 48.78% to 54.35% roof U-value reductions therefore yield only 12.9% to 14.4% envelope reductions, the main practical limitation of a roof-only retrofit. No mat with 10 mm thickness meets the ENS numerical roof criterion of 1.2 W m^{-2} K^{-1}; 24.9 to 31.2 mm would be required, which future measurements will test. On an indicative basis, only the grass shed lies inside the IMAC 80% band, and none lies inside the 90% band, so no comfort acceptability is claimed without validated operative temperature. A first-order scenario suggests that lining the walls with the same 10 mm jute mat could reduce envelope conductance by 58.1%.

The tested 10 mm linings did not provide thermal comfort in GI-sheet labor sheds in a tropical climate. Lining thickness limits the achievable U-value more than fiber type, and roof lining is a load-reduction measure rather than a complete thermal solution for lightweight labor sheds. Untreated mats should not be used in occupied housing until a fire assessment is completed. Longitudinal studies of thicker treated linings, combined with wall insulation and single- or multiple-layer packing methods, are needed to achieve thermal comfort in GI-roof labor sheds.

Author Contributions: Conceptualization, U.V. and R.S.P.; methodology, U.V., R.S.P., G.R.K. and R.S.; formal analysis, U.V., R.S.P., G.R.K. and R.S.; investigation, U.V., R.S.P., G.R.K. and R.S.; validation, G.R.K. and R.S.; visualization, U.V. and R.S.P.; writing—original draft preparation, U.V.; writing—review and editing, R.S.P. and R.S.; supervision, R.S.P. All authors have read and agreed to the published version of the manuscript.

Funding: This research was funded by the Council of Architecture, India, under the Sanshodhan Research Scheme 2025, through the Outcome-Oriented Research Program for Senior Teachers/Architects, grant number CA/345(1)/Sanshodhan/2025.

Data Availability Statement: Data will be made available upon request from the corresponding author.

Acknowledgments: The authors thank SRM Institute of Science and Technology, Kattankulathur, Chennai, India, for providing the necessary research infrastructure.

Conflicts of Interest: The authors declare no conflicts of interest.

Abbreviations

The following abbreviations are used in this manuscript:

ENS	Eco-Niwas Samhita
GI	Galvanized iron
HGR	Heat-gain reduction
IMAC	India Model for Adaptive Comfort
ISO	International Organization for Standardization
MRT	Mean radiant temperature
A	Area (m^2)
E_{st}	Stored energy per unit area (J m^{-2})
c_p	Specific heat capacity (J kg^{-1} K^{-1})
f	Relative amplitude attenuation (-)
f_d	Decrement factor (ISO 13786) (-)
h_c	Convective heat transfer coefficient (W m^{-2} K^{-1})
h_r	Radiative heat transfer coefficient (W m^{-2} K^{-1})
λ	Thermal conductivity (W m^{-1} K^{-1})

L	Layer thickness (m)
P	Period of periodic forcing (s)
n	Number of days or layers (-)
q	Heat flux density (W m^{-2})
Q	Heat transfer rate (W)
R	Thermal resistance (m^2 K W^{-1})
R_{si}	Internal surface resistance (m^2 K W^{-1})
R_{se}	External surface resistance (m^2 K W^{-1})
R_{total}	Total thermal resistance of the assembly (m^2 K W^{-1})
Δt_φ	Periodic time shift (s or min)
Δt_d	Daytime integration interval (s or h)
T	Temperature (°C)
T_{air}	Air temperature in the operative temperature relation, taken as T_{in} (°C)
T_{in}	Indoor air temperature (°C)
T_{max}, T_{min}	Daily maximum and minimum interior-surface temperature (°C)
T_{mrt}	Mean radiant temperature (°C)
T_n	Adaptive neutral temperature (°C)
T_{od}	Daily mean outdoor air temperature (°C)
T_{op}	Operative temperature (°C)
T_{rm}	Outdoor running mean temperature (°C)
$T_{s,in}$	Interior exposed surface temperature (°C)
$T_{s,out}$	Outer surface temperature of the GI sheet (°C)
Z_{12}	Off-diagonal element of the heat transfer matrix (m^2 K W^{-1})
Y_{12}	Periodic thermal transmittance (W m^{-2} K^{-1})
U	Thermal transmittance (U-value) (W m^{-2} K^{-1})
ΔT_{sw}	Diurnal swing of interior-surface temperature (K)
F_c	Ceiling angle factor for a seated person (-)
UA	Envelope conductance (W K^{-1})
X	Measured input quantity
Y	Derived quantity
α	Thermal diffusivity (m^2 s^{-1})
Δ	Uncertainty or difference
κ	Areal heat capacity (J m^{-2} K^{-1})
ε_{st}	Storage share of daytime conducted energy (%)
ρ	Bulk density (kg m^{-3})
τ	Single-capacity thermal time constant (s or h)
Subscripts	
ref, config	Bare GI reference configuration and lined configuration
roof, wall, env	Roof, wall, and whole envelope
i	Index of a layer, input quantity, or day

References

1. Barbhuiya, S.; Adak, D.; Marthong, C.; Forth, J. Sustainable Solutions for Low-Cost Building: Material Innovations for Assam-Type House in North-East India. *Case Stud. Constr. Mater.* **2025**, *22*, e04461. [CrossRef]
2. Amankwaa, E.F.; Roberts, B.M.; Mensah, P.; Gough, K.V. Impact of Roofing Materials on School Temperatures in Tropical Africa. *Build. Cities* **2025**, *6*, 139–157. [CrossRef]
3. Wilby, R.L.; Kasei, R.; Gough, K.V.; Amankwaa, E.F.; Abarike, M.; Anderson, N.J.; Codjoe, S.N.A.; Griffiths, P.; Kaba, C.; Abdullah, K.; et al. Monitoring and Moderating Extreme Indoor Temperatures in Low-Income Urban Communities. *Environ. Res. Lett.* **2021**, *16*, 024033. [CrossRef]
4. Venugopal, V.; Latha, P.K.; Shanmugam, R. Quantifying the Impact of Heat Stress on Labour Productivity in Outdoor Workplaces in Southern India amid a Changing Climate. *Sci. Rep.* **2026**, *16*, 14228. [CrossRef] [PubMed]
5. Berger, T.; Chundeli, F.A.; Pandey, R.U.; Jain, M.; Tarafdar, A.K.; Ramamurthy, A. Low-Income Residents' Strategies to Cope with Urban Heat. *Land Use Policy* **2022**, *119*, 106192. [CrossRef]

6. Pawłosik, D.; Cebrat, K.; Brzezicki, M. Exploring Advancements in Bio-Based Composites for Thermal Insulation: A Systematic Review. *Sustainability* **2025**, *17*, 1143. [CrossRef]
7. Raza, M.; Farhan, A.; Abu-Jdayil, B. Lignocellulose-Based Insulation Materials: A Review of Sustainable and Biodegradable Solutions for Energy Efficiency. *Int. J. Thermofluids* **2024**, *24*, 100844. [CrossRef]
8. Mort, R.; Vorst, K.; Curtzwiler, G.; Jiang, S. Biobased Foams for Thermal Insulation: Material Selection, Processing, Modelling, and Performance. *RSC Adv.* **2021**, *11*, 4375–4394. [CrossRef] [PubMed]
9. *ISO 8301:1991*; Thermal Insulation—Determination of Steady-State Thermal Resistance and Related Properties—Heat Flow Meter Apparatus. International Organization for Standardization (ISO): Geneva, Switzerland, 1991. Available online: https://www.iso.org/standard/15421.html (accessed on 27 October 2026).
10. Panyakaew, S.; Fotios, S. New Thermal Insulation Boards Made from Coconut Husk and Bagasse. *Energy Build.* **2011**, *43*, 1732–1739. [CrossRef]
11. Czajkowski, Ł.; Kocewicz, R.; Weres, J.; Olek, W. Estimation of Thermal Properties of Straw-Based Insulating Panels. *Materials* **2022**, *15*, 1073. [CrossRef] [PubMed]
12. Colinart, T.; Pajeot, M.; Vinceslas, T.; Hellouin de Ménibus, A.; Lecompte, T. Thermal Conductivity of Biobased Insulation Building Materials Measured by Hot Disk: Possibilities and Recommendation. *J. Build. Eng.* **2021**, *43*, 102858. [CrossRef]
13. Shaik, S.; Talanki, A.B.P.S. Optimizing the Position of Insulating Materials in Flat Roofs Exposed to Sunshine to Gain Minimum Heat into Buildings under Periodic Heat Transfer Conditions. *Environ. Sci. Pollut. Res.* **2016**, *23*, 9334–9344. [CrossRef] [PubMed]
14. Iozzino, F.; Fragnito, A.; Mauro, G.M.; Roselli, C. Preliminary Optimization of Steady-State and Dynamic Thermal Performance of 3D Printed Foamed Concrete. *Thermo* **2026**, *6*, 13. [CrossRef]
15. Ferencz, M.; Nagy, B.; Gyenis, J.; Feczkó, T. An Experimental Study on the Thermal Behavior of PCM Plaster-Lined Model House Walls During a Whole Spring Season Influenced by Their Orientation. *Thermo* **2026**, *6*, 23. [CrossRef]
16. Li, F.G.N.; Smith, A.Z.P.; Biddulph, P.; Hamilton, I.G.; Lowe, R.; Mavrogianni, A.; Oikonomou, E.; Raslan, R.; Stamp, S.; Stone, A.; et al. Solid-Wall U-Values: Heat Flux Measurements Compared with Standard Assumptions. *Build. Res. Inf.* **2015**, *43*, 238–252. [CrossRef]
17. Ang, Y.Q.; Sparsh; Wang, T.; Chew, L.W. Low-Cost Interventions for Heat Stress Mitigation in Urban Informal Settlements. *Nat. Cities* **2026**, *3*, 22–27. [CrossRef]
18. Sabapathy, K.A.; Gedupudi, S. On the Thermal Performance of Naturally Ventilated Room with Straw Insulation Retrofitted Envelope for Different Climatic Zones of India. *J. Clean. Prod.* **2022**, *342*, 130665. [CrossRef]
19. Rosa Latapie, S.; Sabathier, V.; Abou-Chakra, A. Bio-Based Building Materials: A Prediction of Insulating Properties for a Wide Range of Agricultural By-Products. *J. Build. Eng.* **2024**, *86*, 108867. [CrossRef]
20. D'Orazio, M.; Maracchini, G. An Experimental Investigation on the Indoor Hygrothermal Environment of a Reinforced-EPS Based Temporary Housing Solution. *Energy Build.* **2019**, *204*, 109500. [CrossRef]
21. Fosas, D.; Moran, F.; Natarajan, S.; Orr, J.; Coley, D. The Importance of Thermal Modelling and Prototyping in Shelter Design. *Build. Res. Inf.* **2020**, *48*, 379–400. [CrossRef]
22. *ISO 8302:1991*; Thermal Insulation: Determination of Steady-State Thermal Resistance and Related Properties: Guarded Hot Plate Apparatus, Edition 1 (Reviewed and Confirmed in 2024). International Organization for Standardization: Geneva, Switzerland, 1991. Available online: https://www.iso.org/standard/15422.html (accessed on 27 October 2026).
23. *ASTM E1269-11(2018)*; Standard Test Method for Determining Specific Heat Capacity by Differential Scanning Calorimetry. ASTM International: West Conshohocken, PA, USA, 2018. Available online: https://store.astm.org/e1269-11r18.html (accessed on 27 October 2026).
24. *ISO 9869-1:2014*; Thermal Insulation: Building Elements: In-Situ Measurement of Thermal Resistance and Thermal Transmittance: Part 1: Heat Flow Meter Method, Edition 1 (Reviewed and Confirmed in 2025). International Organization for Standardization: Geneva, Switzerland, 2014. Available online: https://www.iso.org/standard/59697.html (accessed on 27 October 2026).
25. Choi, D.-S.; Lee, Y.-J.; Moon, J.-H.; Kim, Y.-S.; Ko, M.-J. Estimating In-Situ R-Value of Highly Insulated Building Walls Based on the Measurement of Temperature and Heat Flux Inside the Wall. *Energies* **2023**, *16*, 5714. [CrossRef]
26. *ISO 6946:2017*; Building Components and Building Elements: Thermal Resistance and Thermal Transmittance: Calculation Methods, Edition 3 (Reviewed and Confirmed in 2022). International Organization for Standardization: Geneva, Switzerland, 2017. Available online: https://www.iso.org/standard/65708.html (accessed on 27 October 2026).
27. Bergman, T.L.; Lavine, A.S.; Incropera, F.P.; DeWitt, D.P. *Fundamentals of Heat and Mass Transfer*, 7th ed.; John Wiley & Sons: Hoboken, NJ, USA, 2011.
28. *ISO 13786:2017*; Thermal Performance of Building Components: Dynamic Thermal Characteristics: Calculation Methods, Edition 3 (Reviewed and Confirmed in 2022). International Organization for Standardization: Geneva, Switzerland, 2017. Available online: https://www.iso.org/standard/65711.html (accessed on 27 October 2026).

29. *ISO 7726:2025*; Ergonomics of the Thermal Environment: Instruments for Measuring and Monitoring Physical Quantities, Edition 3. International Organization for Standardization: Geneva, Switzerland, 2025. Available online: https://www.iso.org/standard/78238.html (accessed on 27 October 2026).
30. Manu, S.; Shukla, Y.; Rawal, R.; Thomas, L.E.; de Dear, R. Field Studies of Thermal Comfort across Multiple Climate Zones for the Subcontinent: India Model for Adaptive Comfort (IMAC). *Build. Environ.* **2016**, *98*, 55–70. [CrossRef]
31. *ISO 13789:2017*; Thermal Performance of Buildings: Transmission and Ventilation Heat Transfer Coefficients: Calculation Method, Edition 3 (Reviewed and Confirmed in 2022). International Organization for Standardization: Geneva, Switzerland, 2017. Available online: https://www.iso.org/standard/65713.html (accessed on 27 October 2026).
32. Moffat, R.J. Describing the Uncertainties in Experimental Results. *Exp. Therm. Fluid Sci.* **1988**, *1*, 3–17. [CrossRef]
33. Ramful, R. Thermal Insulation Performance of Natural Fibre-Reinforced Composites: A Comprehensive Review. *J. Renew. Mater.* **2026**, *14*, 7. [CrossRef]
34. El Messiry, M.; El-Tarfawy, S.Y.; Ayman, Y.; El Deeb, R. Development of High-Performance Thermal Insulation Panels from Flax Fiber Waste for Building Insulation. *J. Ind. Text.* **2025**, *55*, 15280837251338160. [CrossRef]
35. Hasan, K.M.F.; Horváth, P.G.; Bak, M.; Alpár, T. A State-of-the-Art Review on Coir Fiber-Reinforced Biocomposites. *RSC Adv.* **2021**, *11*, 10548–10571. [CrossRef] [PubMed]
36. Soussi, Y.; Charai, M.; Oubaha, S.; Mghazli, M.O.; Pfafferott, J.; El Abbassi, F.-E. Climate-Adaptive Hygrothermal Optimization of Heavy Cob Walls Based on Thickness Sensitivity Analysis and TOPSIS Method. *Results Eng.* **2026**, *32*, 112541. [CrossRef]
37. Gopalakrishnan, S.; Shanthi Priya, R.; Law, Y.K.; Fong, C.S.; Senthil, R. Parametric Investigation of Climate-Responsive Roof Design Strategies for Buildings in India. *Eng* **2026**, *7*, 119. [CrossRef]
38. Bureau of Energy Efficiency. *Eco-Niwas Samhita 2018 (Energy Conservation Building Code for Residential Buildings), Part I: Building Envelope*; Section 3.3, Thermal Transmittance of Roof (U_{roof}); Ministry of Power, Government of India: New Delhi, India, 2018; p. 7. Available online: https://beeindia.gov.in/WriteReadData/RTF1984/1772175947.pdf (accessed on 27 October 2026).
39. Athmani, W.; Sriti, L.; Dabaieh, M.; Younsi, Z. The Potential of Using Passive Cooling Roof Techniques to Improve Thermal Performance and Energy Efficiency of Residential Buildings in Hot Arid Regions. *Buildings* **2023**, *13*, 21. [CrossRef]
40. Sigikumar, T.S.; Shafi, K.A.; Thomas, R.J.; Sudheer, A. Experimental Analysis on Heat Mitigation Potential of Stacked Coir Fiber Mat and Perlite as an Alternative for Green Roof. *J. Ind. Text.* **2022**, *52*, 15280837221126190. [CrossRef]
41. Sigi Kumar, T.S.; Shafi, K.A.; Thomas, R.J.; Mohammed, J. Experimental Evaluation of the Thermal Performance of Coir Mat and Green Facade as Wall Insulation in a Tropical Climate. *Therm. Sci. Eng. Prog.* **2023**, *40*, 101757. [CrossRef]
42. Cigarruista Solís, L.; Chen Austin, M.; Deago, E.; López, G.; Marin-Calvo, N. Rice Husk-Based Insulators: Manufacturing Process and Thermal Potential Assessment. *Materials* **2024**, *17*, 2589. [CrossRef] [PubMed]
43. Vimalraj, A.; Jeyasubramanian, K.; Baskar, I. Sustainable Building Envelopes: Evaluating the Thermal Performance of Thatched Roofs Fabricated Using Coconut Leaves. *Sustain. Chem. Pharm.* **2024**, *42*, 101771. [CrossRef]
44. Palumbo, M.; Lacasta, A.M.; Giraldo, M.P.; Haurie, L.; Correal, E. Bio-Based Insulation Materials and Their Hygrothermal Performance in a Building Envelope System (ETICS). *Energy Build.* **2018**, *174*, 147–155. [CrossRef]
45. Jensen, N.F.; Møller, E.B.; Hansen, K.K.; Rode, C. Hygrothermal Assessment of Three Bio-Based Insulation Systems for Internal Retrofitting Solid Masonry Walls. *J. Build. Phys.* **2024**, *48*, 244–280. [CrossRef]
46. Sayam, S. Natural Fibers in Sustainable Materials: Extraction Technologies, Fiber Modification, and Performance-Sustainability Relationships. *RSC Adv.* **2026**, *16*, 10495–10537. [CrossRef] [PubMed]
47. Oladele, I.O.; Oki, V.O.; Bichang'a, D.O.; Agbeboh, N.I.; Makinde-Isola, B.A.; Abraham, O.F.; Borisade, S.G. Effects of Constituents and Morphology on Durability of Plant-Based Cellulosic Fibers and Their Composites: A Review on Sustainable Biocomposites Materials. *Next Sustain.* **2026**, *7*, 100283. [CrossRef]
48. Yang, Y.; Haurie, L.; Wang, D.-Y. Bio-Based Materials for Fire-Retardant Application in Construction Products: A Review. *J. Therm. Anal. Calorim.* **2022**, *147*, 6563–6582. [CrossRef]
49. Hernández-Pérez, I. Influence of Traditional and Solar Reflective Coatings on the Heat Transfer of Building Roofs in Mexico. *Appl. Sci.* **2021**, *11*, 3263. [CrossRef]
50. Central Electricity Authority. *CO_2 Baseline Database for the Indian Power Sector: User Guide, Version 20.0*; Ministry of Power, Government of India: New Delhi, India, 2024. Available online: https://cea.nic.in/api/cdm-report-version/view-pdf/en/76 (accessed on 27 October 2026).

Disclaimer/Publisher's Note: The statements, opinions and data contained in all publications are solely those of the individual author(s) and contributor(s) and not of MDPI and/or the editor(s). MDPI and/or the editor(s) disclaim responsibility for any injury to people or property resulting from any ideas, methods, instructions or products referred to in the content.